4-1-2022

System Design and Control Optimization for Neurorehabilitation Exoskeleton

Rodrigo N. Ramon
Florida International University, rramo066@fiu.edu

Recommended Citation
Ramon, Rodrigo N., "System Design and Control Optimization for Neurorehabilitation Exoskeleton" (2022). *FIU Electronic Theses and Dissertations*. 4937.
https://digitalcommons.fiu.edu/etd/4937

FLORIDA INTERNATIONAL UNIVERSITY

Miami, Florida

SYSTEM DESIGN AND CONTROL OPTIMIZATION FOR NEUROREHABILITATION EXOSKELETON

A dissertation submitted in partial fulfillment of the
requirements for the degree of
DOCTOR OF PHILOSOPHY
in
ELECTRICAL AND COMPUTER ENGINEERING
by
Rodrigo Nicolas Ramon

2022

To: Dean John L. Volakis
College of Engineering and Computing

This dissertation, written by Rodrigo Nicolas Ramon, and entitled System Design and Control Optimization for Neurorehabilitation Exoskeleton, having been approved in respect to style and intellectual content, is referred to you for judgment.

We have read this dissertation and recommend that it be approved.

Jean Andrian

Hai Deng

Aparna Aravelli

Ou Bai, Major Professor

Date of Defense: April 1, 2022

The dissertation of Rodrigo Nicolas Ramon is approved.

Dean John L. Volakis
College of Engineering and Computing

Andrés G. Gil
Vice President for Research and Economic Development
and Dean of the University Graduate School

Florida International University, 2022

DEDICATION

To my parents.

ACKNOWLEDGMENTS

My sincere and endless gratitude to my advisor, committee, colleagues, supporting faculty, friends, and family, without whom the completion of this work would not have been possible.

I offer my deepest thanks and appreciation to my primary advisor and mentor, Dr. Ou Bai, for being a beacon of knowledge, support, patience, and understanding throughout my academic journey. Thank you for being consistently accessible and willing to offer your guidance at every opportunity, without hesitation.

I would be remiss to not mention or offer my sincere thanks to Dr. Jean Andrian, Dr. Aparna Aravelli, Dr. Hai Deng, and Dr. Edgar Vieira for their essential insight, time, and aid throughout this process.

I would also like to acknowledge my Human Cyber-Physical Systems lab colleagues and friends, who were unwavering sources of assistance, humor, and support: Roozbeh, Sebas, Masud, Tushar, Robin, and Connie.

A special thanks to my best friend, Fidel, who has always been there for me through every challenge and obstacle in my path.

To my beautiful Monica, I never would have gotten this far without your help. In every way, I thank you, and I love you.

This research was supported by the McKnight fellowship, and the Florida Georgia Louis Stokes Alliance for Minority Participation (FGLSAMP) fellowship, funded by the National Science Foundation.

ABSTRACT OF THE DISSERTATION

SYSTEM DESIGN AND CONTROL OPTIMIZATION FOR NEUROREHABILITATION EXOSKELETON

by

Rodrigo Nicolas Ramon

Florida International University, 2022

Miami, Florida

Professor Ou Bai, Major Professor

Neurorehabilitation is a comprehensive approach aimed at helping patients regain motor control after a neural injury, including spinal cord injury, stroke, or other ischemic events. Early-stage neurorehabilitation is particularly delicate due to voluntary muscular weakness and lack of motor control, presenting in the form of spasticity. Unfortunately, this period of elevated weakness is when most neural control improvement can be made through a phenomenon called brain plasticity. Early rehabilitation traditionally requires a human therapist due to the adaptive and dynamic interpretation of undesired neuromuscular events. While efforts have been made to develop devices to aid in neurorehabilitation, the considerations that must be taken into account to design and develop an applicable, effective, and safe device can become a hindrance, preventing the proliferation of devices that could affect positive change in the communities that require them. Considerations for a neurorehabilitation device include sensor placement and usage, mechanical design, control system and design, physical interfacing, and user experience. In the following work, we first explore the physical design and development of an exoskeleton-type device, funded by the Department of Energy, that provides active assistive support to users and is therefore adaptable for early-stage neurorehabilitation patients. This device is capable of singular joint movement using a position-following controller with a manual interface. We employed serial elastic actuating modalities to stabilize displacement sensations and provided joint space feedback required for accurate displacement. We further include an analysis into control efficacy, wherein the average settling time for the position-based algorithm was of 2.02s, and the velocity algorithm performed at 3.04s. In terms of accuracy, the users were able to reach the desired positions within the 10 second time limit with 81% and 73% accuracy for the position control and velocity control, respectively. Following, we explore control mechanisms applicable to rehabilitative devices and define an admittance controller. We conclude parameterized control using biomechanical signals in an exoskeleton-type is viable, and including a feed-forward loop in the admittance controller provides the most coupled stability in the system following marginal analyses.

TABLE OF CONTENTS

CHAPTER PAGE

LIST OF FIGURES

LIST OF ABBREVIATIONS

CDC	Centers for Disease Control and Prevention
EMG	Electromyography
IMU	Inertial Measurement Unit
SCARA	Selective Compliance Assembly Robot Arm
MVC	Maximum Voluntary Contraction
PID	Proportional-Integral-Derivative (Controller)
PI	Proportional-Integral (Controller)
PD	Proportional-Derivative (Controller)
LTI	Linear time invariant
DOF	Degree of freedom

CHAPTER 1

INTRODUCTION AND BACKGROUND

1.1 Stroke and Neural Injury

Strokes and spinal cord injuries are the leading causes of serious long-term disability [1]. Every year, nearly 800,000 people suffer a stroke, and stroke alone is the primary source of long-term disability in the United States [1]. Neurologically debilitated persons are then burdened with handicaps in the form of motor impairments, usually in the form of hemiparesis. Mechanically, strength, range of movement, and dexterity are all affected by these events, leading to loss of function, self-reliability, and confidence [2, 3]. However, some degree of rehabilitation can be obtained through neurorehabilitative therapy, which aims to rehabilitate damaged synapses debilitated by traumatic brain injury, spinal cord injury, or cerebrovascular events [4].

Traditional Rehabilitation

Neurorehabilitation is similar to physical rehabilitation in that both contain a physical component of movement, however the method is completely different [5]. Neural therapy focuses on exploiting a phenomenon referred to as brain plasticity, where therapists can elicit a cognitive response, thereby emphasising the neurological component of human locomotion [6]. Stroke recovery is subjective, depending on a variety of factors including whether it is the patient's first stroke, the location of the stroke within the brain, and the severity and duration of the event, among others [7]. Shown in Fig. 1.1 [8] in terms of recovery and functional ability, the recovery process can be divided into three stages: the acute stage, starting at the event and covering the first few days; the sub-acute phase, commencing after the first few days have passed; and the chronic stage, which begins after a few months have passed

[8, 9]. Patient outcomes have been largely attributed to rehabilitation exposure early and often during the patient's weakest state, requiring extensive care and oversight [10]. Established research shows that these patients tend to experience a plateau of improvement approximately 6 months after the initial injury [11]. Therefore, it is critical to initiate therapy as early as possible while providing the maximum possible rehabilitation exposure to patients.

Barriers

We interviewed multiple local neurorehabilitation centers and asked where their primary struggles currently lie; they stated a lack of physical labor force and workforce bottlenecks. These centers usually deal with older patients, often overweight, who cannot ambulate properly and rely on therapists as the main source of support. For these critical months, therapists are required to provide full motor movement support while verbally guiding the patient, and monitoring and correcting unwanted phenomena such as spasticity and compensatory movements [12]. The overall limiting factor for the ubiquity and availability of these services is the current requirement for a trained therapist to be present and fully concentrated on the patient, and the fatigue that comes from the mechanical movements, creating a workforce bottleneck. This bottleneck affects the outcomes of patients in that therapists can only see so many patients if they can only work with one at a time [11]. Therefore, patients receive a lower frequency of therapy sessions, thereby directly limiting the possible rehabilitation exposure they require to regain their faculties.

In addition to workforce problems, the neurological component presents unique circumstances in regards to documenting progress and data collection. Traditional rehabilitation techniques revolve around the patient's repetition of physical movements with several different types of aids with hope that the withered neurological

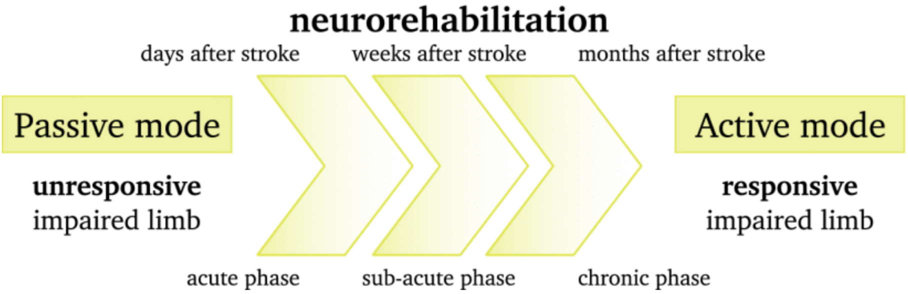

Figure 1.1: General neurorehabilitation timeline. Robot controllers should adapt to the correct phase of the therapy of the stroke survivor. Passive and Active are traditional terms to indicate the involvement of the subject in the training. Image credit [8]

connections will adapt to the existing damage or repair the damaged tissue. In order to do this, instructions for the patient include the aforementioned physical therapy paired with mindfulness to elicit neurological involvement. The problem with this method is the neurological reconditioning is not physically observable. Quantifiable measures of improvement can come from assessment tools such as the Barthel index, which accounts for subjective observations generalized and scaled from 1-10, including categorizations such as feeding, bathing, grooming, etc., [4]. These measures, though useful in a conventional sense, do not take into consideration the full spectrum of development and neurological involvement in progressing patients.

1.2 Rehabilitation Robotics

Research in the last decade has ballooned with robotic solutions to therapeutic problems [13, 14, 15], although not without challenge [16]. There have been many attempts to mitigate the physical labor of neurorehabilitation, and many different interpretations and approaches to reach a solution [17, 14, 15]. We need to categorize these solutions into mechanical and control categories, because neither the mechanical approach nor the control algorithms used are universal. Mechanically, we can categorize rehabilitation devices into exoskeleton-type devices, which function as a supportive structure which parallels the human limb, and external manipulators, referring to actuated robotic devices which provide their actuation from an outer static point. A prominent example of an external manipulator is the MIT-developed MANUS [18] shown in Fig. 1.2 [18], which uses planar movement trajectory-correcting where the patient is sat in front of a table with an actuated handle using a screen as visual feedback for coordination tasks [19]. The MANUS has been in development since 1992 and consists of a Selective Compliance Articulated Robot Arm (SCARA) device, with an impedance-based controller that reads a force sensor at the handle that needs to be triggered by the patient [20]. The MANUS accentuates the perceived motion and then provides visual feedback, allowing the patient to attempt to error-correct their initial motion [20]. The device was designed to be highly backdriveable, and originally was designed with a wrist recovery module that was phased out of future versions [20]. As will be detailed in Chapter 4, impedance control is beneficial in some scenarios but does not modulate the provided assisting force and relies on impulse-based movement assistance triggered by the user. The MANUS, however, has been shown to provide some benefit [19] to patients, and has had a vertical movement module subsequently developed for it [18].

Another external manipulation device is the MIME [21], which uses bi-manual slave-master SCARA manipulators to perform a kind of mirror therapy for neural recovery. As shown in Fig. 1.3 [21], the MIME consists of one actuated 6-degrees of freedom (DOF) robotic manipulator PUMA-560, normally intended for industrial applications such as welding, paired with a 6-DOF position digitizer to record the patient's healthy hand and provide mirrored actuation. The MIME was designed with a position-based controller which reads the position input of the digitizer. The

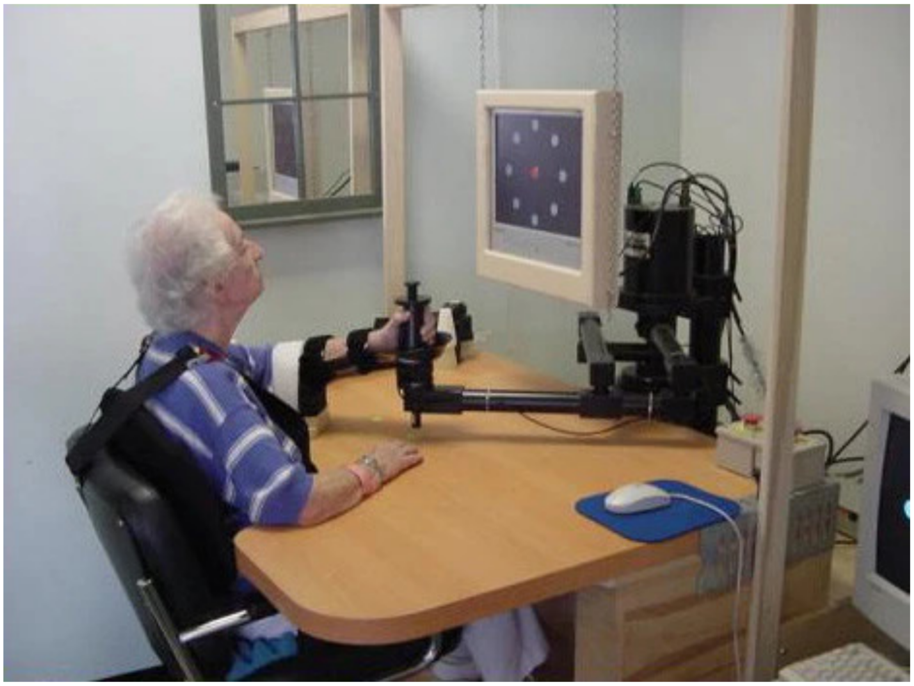

Figure 1.2: MANUS device. Pictured is the SCARA arm holding the force sensor in the handle, with the visual feedback screen located above the table. Image credit [18]

PUMA-560 copies the movement and moves the patient's affected arm in sync with the unaffected arm. The MIME is capable of providing assistance to hemiparetic patients to undergo mirror therapy, and has since been developed to include different control methodologies to assist in various therapeutic needs, such as resistive movement and movement trajectory correction based on preset paths. The MIME robot excels at the task it was designed to do, but is less capable than the MANUS in its ability to adapt to new tasks, as the designed input is very specific to hemiparetic patients with a healthy limb.

External manipulation devices tend to be fixed to a singular location, with patients being brought to the machine as needed. This can create logistical complications with some patients as the machine cannot be brought to them. Exoskeleton devices, however, do not require the device to be mobile. The Lokomat, shown in

Figure 1.3: MIME device using bilateral assisted movement. The patient's left arm is attached to the position digitizer for mirror therapy. Image credit [21]

Fig. 1.4 [22], is a robotic treadmill training station comprising of a treadmill and stationary exoskeleton to provide the physically laborious task of manipulating the patient's leg(s) as they walk [23]. The Lokomat's exoskeleton is hung by the hips on the treadmill, which then operates in tandem with the leg movements. The control of this exoskeleton, however, is fixed and unaware. Clinical operation of this device is strictly position-based with preset trajectory following with no force feedback or biofeedback otherwise [22]. This control approach would fail to identify possible spasticity and muscular misfiring, and could result in serious physical damage and pain to the patient. Mechanically, the Lokomat is a large station which requires fixed installation, and therefore suffers the same limitations as many external manipulation devices.

Mobile exoskeleton devices are more ergonomic and provide more adaptability to a variety of tasks, whereas purpose-built devices have a more limited range of potential use or adaptability. Exoskeleton devices may be utilized in support of: the

Figure 1.4: Lokomat device using exoskeleton device on treadmill. Image credit [22]

upper body, such as the ARMIN [24], which uses an impedance controller framework and a large stationary frame with a single arm 6-DOF chassis with 4 active and 2 passive joints; the lower body, such as the ExoAtlet [25], which is mobile and can be adapted to a variety of tasks but does not account for biomechanical feedback for its operation; or dedicated to hand and finger recovery such as the AMES [26], which uses an impedance controller with visual force feedback for patient self-correction and provides vibrations to lengthen and relax muscular contractions of spastic origin. The efficacy of these devices has been supported [27, 28] in a variety of contexts and has proven to be a worthwhile tool to assist in rehabilitating those with neural ailments.

There have been a variety of planar movement devices, vertical movement devices, passive devices, active devices, and exoskeleton devices, among others. Some

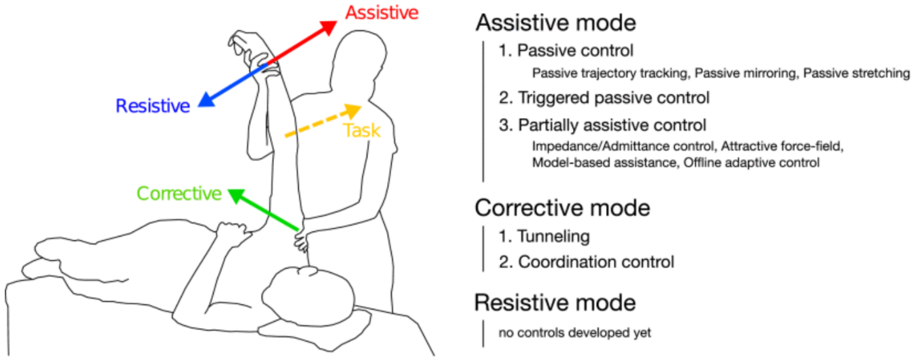

Figure 1.5: Three global strategies for robotic-mediated rehabilitation and the current implementations on robotic exoskeletons. Image credit [8]

common control modes used can be seen in Fig. 1.5 [8]. Resistive assistance does not directly apply, as this is a mode of operation that requires advanced neuromuscular control, and is not applicable to early-stage rehabilitation patients. Some of these devices have had clinical success and some have even been commercialized.

1.3 Bio-signal Background

The requirement for an exoskeleton device to have environmental awareness is paramount for safe and smart operation. We wish to determine which bio-signals we may employ here to provide a naturally intuitive mode of interface which provides the robotic device reliable and accurate information about the environment it is in, and how it is desired to actuate. In the field of rehabilitation robotics and exoskeletal robotic aids, determining user intent and then reproducing said intent based on limited information is critical to produce a system which can fulfill the needs defined by the nature of the robotic arm. Understanding user intent is critical in the accurate replication of these movements by any robotic entity. It is natural to consider exoskeleton movement mirroring human locomotion. Since muscular contractions enable human locomotion, muscular activity can be monitored to trigger a movement. Additionally, kinetic and kinematic signals attained from limb locomotion are bio-signals as well. These signals include kinetic data based off force/torque sensors, position/movement data from encoders and inertial measurement unit (IMU) modules.

1.3.1 EMG in Robotics

Surface electromyography (EMG) involves the superficial adhesion of electrodes to extract the electric potential triggered either electrically or neurologically. Collecting and studying features of these signals is not only an accurate way to allow for precise mechatronic replication, but also to accurately gauge muscle involvement by recording and comparing EMG signals from different stages of the rehabilitation process. Studies have been carried out to determine the EMG muscles responsible for upper limb locomotion [29, 30, 31, 32, 33]. Fig. 1.6 details the muscles most involved in elbow kinematics. A study by Gupura et. al. [34] summarizes arm movements and their corresponding responsible muscle synergies. Further studies investigate the correlation between EMG and musculoskeletal movements and its feasibility [35]. The works detailed by Koo et. al. [35] describe several neuromusculoskeletal models for the replication of dynamic movement in the elbow. To explore and assess the viability of this approach, works have been performed to correlate maximum voluntary contraction (MVC) force and EMG depending on the joint angle, specifically the elbow [36]. The information derived displays a direct correlation in joint angle and MVC force has proved to be insignificant. Non-linear regression methods, linear regression methods, and polynomial methods can be employed to model the position signal.

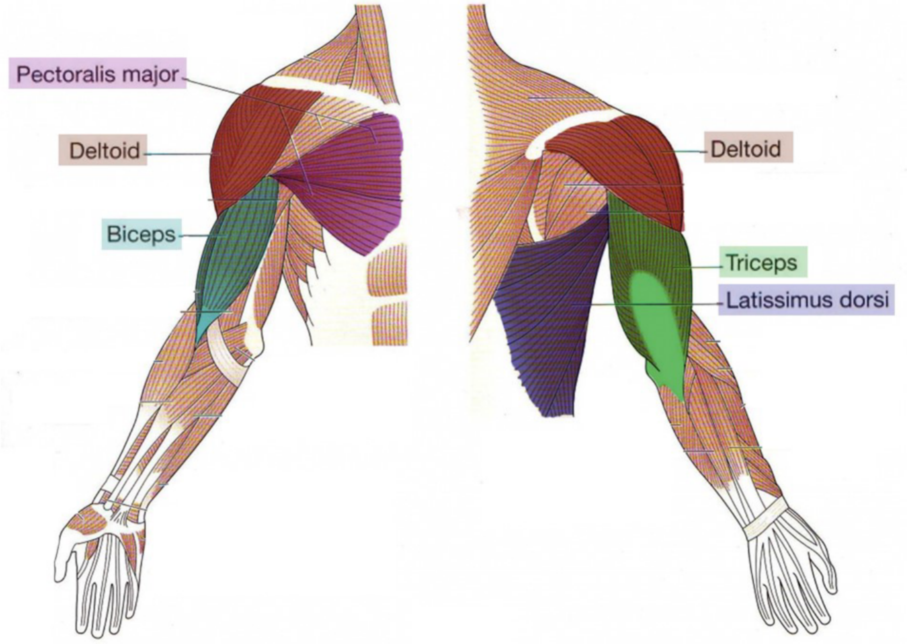

Figure 1.6: Diagram of frontal (left) and back (right) muscles primarily elbow flexion and extension

1.4 Motivation

While research shows that strides are being made to propagate this robo-therapy, development considerations and the entwined effects of control considerations, actuating devices, sensors, and even chassis design of such a device contain no standards for effective design, whether that be in control methodology, mechanical design, or sensor usage. We discuss the benefits of admittance control and describe the process of stabilizing the system, margins of operational feasibility, the limitations imposed by mechanical considerations, and requirements imposed by design choices. In order to recognize and assess critical design considerations, the following questions were addressed:

1. Can we design and manufacture a device that meets the needs of an acute stroke neurorehabilitation patient?

2. Can we improve system control with a proportional-derivative (PD) controller?
3. Can we provide accurate torque modulation using an admittance control system providing accurate, reliable, and stable actuation?

CHAPTER 2

WORKER ASSISTIVE ROBOTIC EXOSKELETON DESIGN AND CONTROL

2.1 Introduction

Workers who perform hotcell manipulation tasks are subjected to long hours of repetitive stationary work that includes constant manipulation of dangerous radioactive materials. A Department of Energy (DOE) sponsored study conducted by the Los Alamos National Laboratory reported the incidence rate of repetitive stress injuries increased from 22% after 1-2 hours of work to 50% after 3 hours of work per day due to fatigue, repetitive motion, and hyper-extension during manipulation tasks in glove-box and hotcell work spaces at DOE facilities [37]. Worker fatigue is a serious topic not only in terms of safety and efficiency of the worker, but also when considering at risk tasks which require the worker to handle dangerous materials, extending the risk to surrounding workers as well. A good example of this danger is hotcell work, which inherently requires heightened focus and care to avoid incidents or injuries. Worker assistive exoskeleton devices have been developed and have recently become commercially available [38, 39]. While these devices aim to assist workers by alleviating muscular strain from repetitive or strenuous tasks, these devices are usually cumbersome. Though they may be ergonomic and comfortable, the geometry of these devices does not account for the restricted space inside the hotbox glove and is therefore rendered unfit.

2.2 Design Requirements and Limitations

Hotcell and Glove Considerations

The nature of an exoskeleton device requires for the device to parallel human movement as naturally as possible. Upper limb movements become more complex the closer you move to distal extremities. The manipulation tasks requiring assistance involve the use of various degrees of freedom, including shoulder horizontal and vertical flexion, abduction and adduction, elbow flexion and extension, and wrist flexion and extension, rotation, and supination. While there exist various worker assistance devices aimed at alleviating worker fatigue in manufacturing and logistics, these devices are meant to be worn by a user without spatial limitations found in a hotbox environment. In addition to this, any communication would be limited to hardwired communications, due to security restrictions within the federally operated nuclear facilities. The glove box in which the exoskeleton needs to operate can impose severe constraints, both physical and visual, on the operator. There are physical and visual limitations on the reaches and restrictions of how someone can sit or stand and of the movement and range of the arms, hands and fingers. This often leads to the operator using an awkward limb movement to complete the task. The standard glove box, also known as a dry box, has a small 10” diameter hole 46” off the ground in which the arm is inserted up to the mid-bicep. The glove in which the arm is inserted starts at 10” and constricts until there is very limited to no space from the mid forearm through the hand, depending on the occupant. The glove itself is a Polyurethane/Chlorosulphonated dry box glove with a 25N tear resistance and 120 °C temperature constraint, with a recommended operational temperature between 5 and 25 °C. The length in which the arm can be extended before stretching of the glove occurs is 30” from the glove port. This means the exoskeleton will have to take up an already very limited space inside the glove area and will have to account for the tearing and heat restrictions of the glove, while still allowing ergonomic movement of the arm during awkward complex movements mid-bicep.

2.2.1 Task Descriptions and Decisions

Through various sources including discussions with specialists and technicians from the Savannah River Site Nuclear Reservation and review of recordings of technicians performing common hotcell tasks, preliminary tasks were developed for the development and assessment of the purposed exoskeleton assistive device. The nature of these tasks is a repetitive and methodical one. Workers often find themselves cleaning radioactive scrap and contaminated materials from deconstructed facilities, as well as packaging and containing various materials such as sands and other loose debris. With this understanding, the decision to produce two tasks simulating common movements was derived.

The first task includes the collection and deposit of loose material represented by sand and involves the subject using a small metal cup to collect debris from a container and collecting it in an adjacent container. The second task represents the cleaning tasks, where the worker is required to clean various large slabs of material, be they of metal, cement, plastics, etc. This task requires the subject to brush a representative brick several times in a repetitive manner, cycling through several bricks in fixed positions while holding a hand brush. This task is repeated for a set amount of time, which was previously determined to assure muscular fatigue. Previous work on this project involved various muscular fatigue identification recordings and calibrations, wherein electromyography (EMG) data was recorded from various

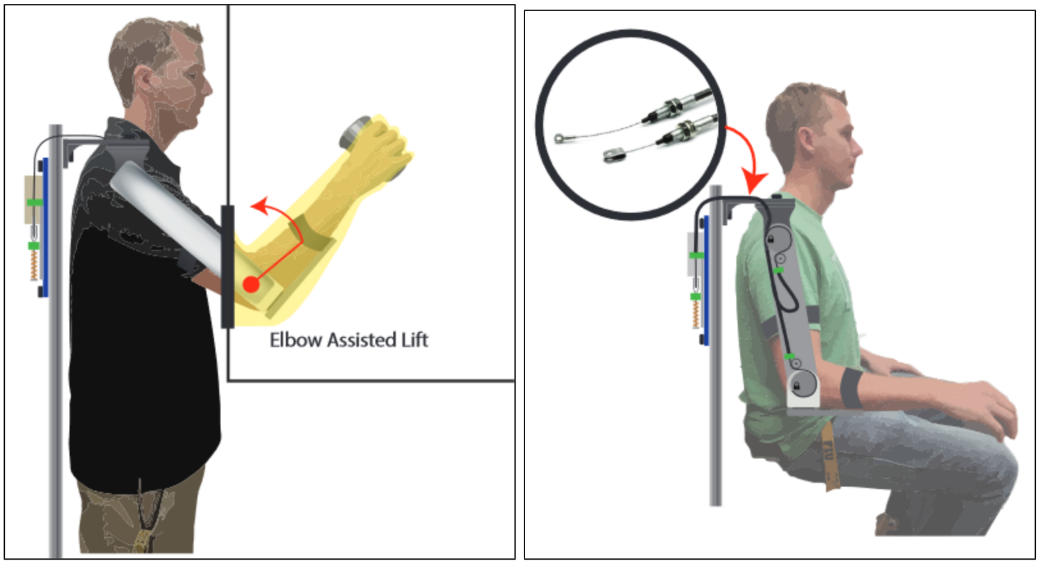

Figure 2.1: Different views of proposed design showing functionality (left) and internal anatomy (right). The images show the use of a Bowden cable to actuate assistance

subjects while performing these tasks to determine varying proponents of fatigue, as well as the locations of primary fatigue.

2.3 Device Specifications and Development

The developed device focuses on major muscular involvement reduction through weight offset and active assistance. The exclusive functioning environment of the device is within a hotcell glove, which as previously discussed, poses various restrictions as far as space and thermal conditions. For this reason, the device must be not only slim and unobtrusive, but must also contain a minimal amount of operating electronics such as motors. Due to these limitations, a device was derived consisting of several joint links and containing both passive and active joints. As mentioned, the device's primary function is to minimize muscular expenditure, which has been observed to consist primarily of deltoid anterior and biceps femoris activation. These muscles are responsible for the arm's ability to maintain and change height. While horizontal movement is required in almost all discussed tasks, sufficient muscular expenditure has not been observed to stem from these horizontal movements, and will therefore be allowed to continue moving freely with no assistance. The current device's degrees of assistance are in the form of elbow flexion and shoulder vertical flexion, with an active assistance component and a passive assistance component, respectively. The elbow flexion assistance device consists of a series spring linear actuator composed of a Maxon Exoskeleton Joint device which rotates to tangentially pull a metal Bowden cable attached to another pulley, which is fixed at the elbow rotation axis. The passive shoulder assistive component shares the basic anatomy of the elbow, however there is no motor involvement to assist in movement, as the assisting force will be provided by a series spring attached to the Bowden cable to allow for passive proportional force to assist with arm lifting, as illustrated in Fig. 2.1 and Fig. 2.2. In addition to these two degrees of freedom, the arm will also be allowed horizontal rotation both in the elbow and shoulder by a free rotating interface consisting of bearings to ease displacement. The links are designed to be constructed of aluminum 2024, due to this alloy's strength and lightweight properties. To minimize the number of components that need to be contained inside the hotbox environment, as well as in the glove, the Bowden cables are led outside the glove, guided through the arm links, and then actuated on from the outside of the hotbox, behind the worker. This allows for full functionality while maintaining the active components in the glove to a minimum. The glove materials, as well as the nature of the flexible glove, have to be considered, as the materials in the hotbox are assumed to be radioactive and highly dangerous. Including a motor for direct drive within the glove was determined to be undesirable and dangerous to the user.

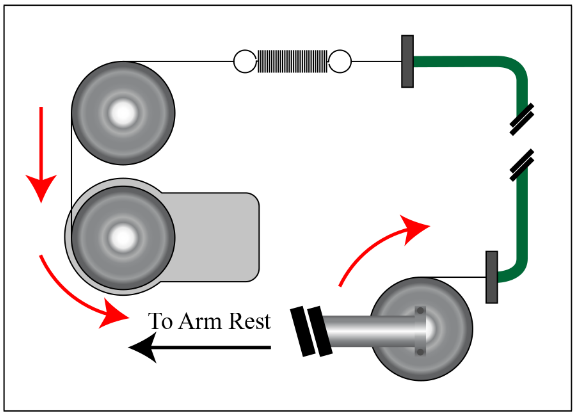

Figure 2.2: Arm actuation mechanics for the active elbow joint assistance mechanism. Displays assistive directional movement transfer, including the series spring

2.4 Assisted Movement Control

Active assistance is required to allow for dynamic movement and muscular involvement minimization to occur concurrently. This goal is to be achieved through various solutions which are currently under development. Initial recordings under controlled conditions have been conducted to calibrate the system dynamics to allow for optimal movement trajectories. In order to initiate movements, a preliminary user initiation switch is set to be triggered by the user when they wish to lift their arm. The system drive consists of a Maxon Exoskeleton Drive, controlled via a 1.2GHz Raspberry Pi 3 Model B with 1GB RAM, programmed in C++. The controller is based on the proportional– integral-derivative (PID) position controller gains, which remains the most widely used industrial controller. The PID controller is simple and easy to understand and requires no preconditions such as accurate system models in use, making it the most widely used controller [38].

Experimental Tests

Position control of the arm is implemented through the PID position controller gains of the Maxon EPOS4 controller. Initial tests were conducted to assess natural human arm motion range and velocity during the desired tasks. These recordings facilitated the understanding of the expected hand movement, and was therefore instrumental in deriving motor movement expectations. Through the test of healthy subjects, the results show the human body can comfortably act while assistance takes place.

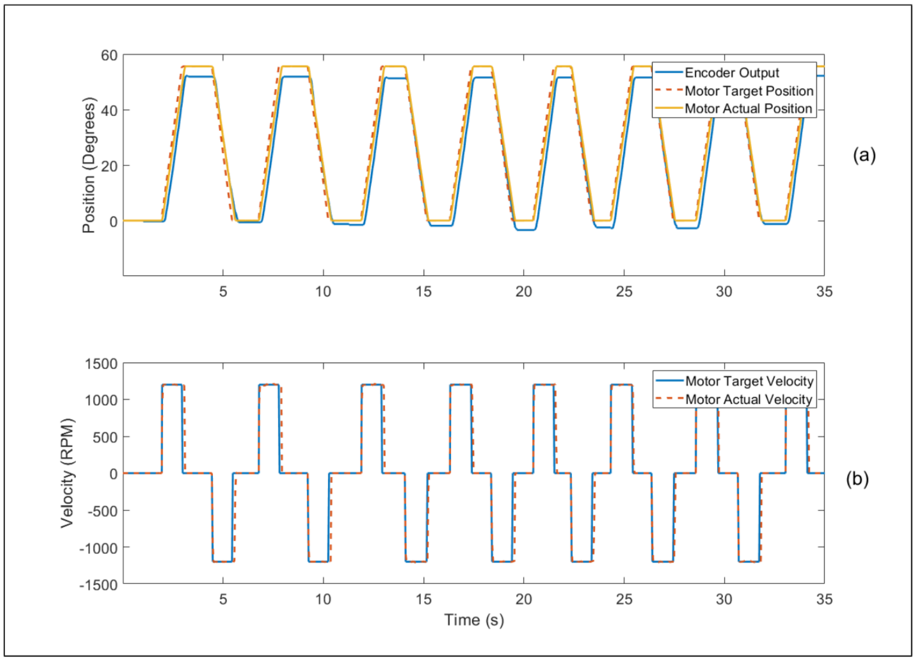

Figure 2.3: Unweighted system response to actuation. Comparison of elbow joint output, target position and actual position (top). Comparison of target velocity and actual velocity (bottom)

Control Design and Identification

In the absence of load in the human hand, the motor drives the human arm to reciprocate through the control system. Fig. 2.3 shows the pre-set speed of the motor and its actual running speed. The two lines almost coincide, indicating the speed error is small and negligible. Similarly, where the subject has a load of 2.5 pounds with no muscular involvement from the subject, the damping spring begins to function and the amplitude of the position output increases, which is shown in Fig. 2.4. A position following controller was applied to the arm motor, shown in

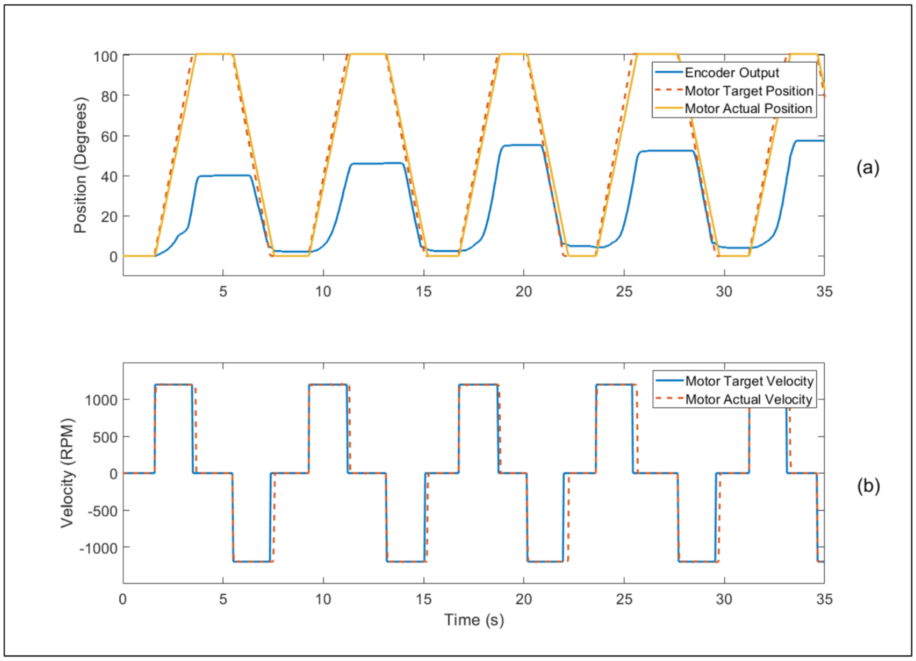

Figure 2.4: Weighted system response to actuation. Comparison of elbow joint output, target position and actual position (top). Comparison of target velocity and actual velocity (bottom)

Fig. 2.3 for unweighted and Fig. 2.4 weighted, showing the conditional differences in the control performance based on the available feedback data. The arm is subjected to a force provided by the series spring in the system. In other words, the shock damper reduces the impact of the load on the subject, and the spring inside it accumulates energy. The spring force helps lift the arm by dissipating energy. The final system allowed the subjects to perform their tasks without hindrance while providing support and assistance throughout.

2.5 Discussion

The mechanical and electronic design of exoskeleton devices need to be purpose-driven and meet specific design requirements based on their intended tasks. For the proposed design, the design specifications required in such a device included:

low temperature, low profile, cable-driven, and comfortable to use. To fulfill the specified requirements, we designed an exoskeleton system to provide assistive force to human users. We were able to provide adequate assistance to users to facilitate reaching tasks, showing the device interface to be intuitive, ergonomic, and effective in providing assistance as the user required it, while meeting the thermal, space, and comfort considerations. The Bowden cable solution employed allowed for actuation at a distance providing the mechanical flexibility needed to traverse the glove and provide assistance for a variety of purposes. Applications for this device also include neurorehabiliative scenarios, although the material construction of this particular prototype requires further mass reduction by employing lighter or more optimized materials. Further works will include feed-forward control implementation and calibration techniques to allow for comprehensive assistive control. In addition, further work will aim to minimize hardware components to simplify the mechanisms required for the systems to properly function, reducing the space needed both in the hotcell, and in the glove contained therein. Although the application may vary vastly, the mechanical design, sensor placement, drive mechanism, and electrical development of this device is in direct support of our neurorehabilitation efforts, as it provides a platform on which to prototype and develop control solutions going forward. This control configuration would adequately meet our requirement of providing active assistive support for early-stage neurorehabilitation patients which require complete assistive movement, as they have no effective muscular toning.

CHAPTER 3

IMPROVED ADAPTIVE SYSTEM CONTROL IN EXOSKELETON DESIGN FOR WORKERS

3.1 Introduction

Following the work completed in chapter 2, control improvements were required to minimize the variance between free and coupled movement. In the following work, an adaptive control system was implemented and tested using a position following controller as well as a velocity following controller. Background and introductory information common to both works is omitted here to minimize redundancy.

3.2 Assisted Control Design

Active assistance is required to allow for dynamic movement and muscular involvement minimization to occur concurrently. This goal is to be achieved through various solutions. Initial recordings under controlled conditions have been conducted to calibrate the system dynamics and allow for optimal movement trajectories. In order to initiate movements, the user is asked to press a button on a provided joystick controller switch, set to be triggered by the users when they wish to lift or lower their arm. The system drive consists of a Maxon Exoskeleton Drive controlled via a 1.2GHz Raspberry Pi 3 Model B with 1GB RAM and programmed in C++. The controller is based on the proportional–integral-derivative (PID) position controller gains, which remains the most widely used industrial controller [40]. Since the PID controller requires no preconditions, such as accurate system models in use, it is simple and easy to understand. Two primary high-level control algorithms were tested under the same conditions.

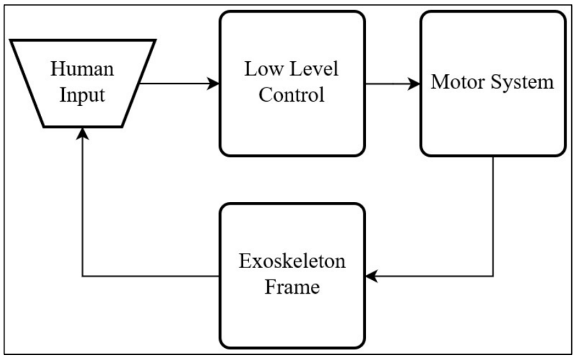

Figure 3.1: Position control algorithm block diagram

Position Control

During position-based control of the system, the input signal of the system is generated via button presses that represent the up and down movement of the arm. The system has two control modes: the high-level controller is for the encoder, and the low-level controller is for the motor. The high-level controller produces the ideal encoder position step, which is tracked by the low-level controller. At the same time, the low-level controller uses the error of the encoder feedback, the system phased run-time interval, and the coefficient to generate an ideal motor speed, which is then passed to the motor system to complete the operation of the entire system. The algorithm block diagram is illustrated in Fig. 3.1. In general, the control sys-

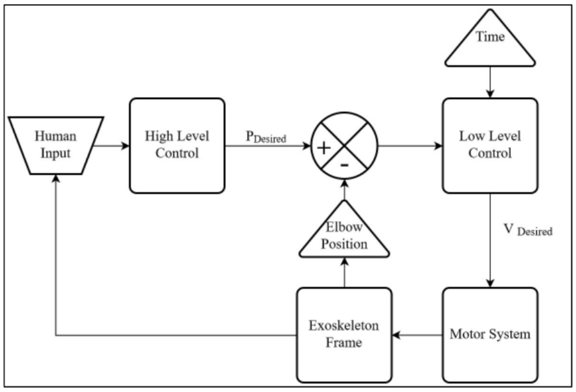

Figure 3.2: Velocity control algorithm block diagram

tem converts the incremental change of the encoder into its angular variation. The encoder-motor ratio is one-to-one, and it feeds back the angle at which the human arm moves up and down. If the position of the encoder feedback is within the preset range of the human body's motion trajectory, the motor will rotate according to the corresponding input signal to meet the subject's requirements so that the arm reaches the ideal position. During this process, the rotation of the motor is achieved by speed control. Its speed is proportional to the feedback error of the encoder. This error is calculated based on the difference between the actual position of the encoder and the desired position of the operator.

Velocity Control

The velocity control, shown in Fig. 3.2, does not contain a high level control layer to determine positions, unlike the position control schema. The motor rotates according to the set fixed speed, which can be subjectively selected by the operator. When the motor stops, if the exoskeleton frame is offset due to some factor, the motor will automatically adjust by the feedback of the encoder to keep the frame position stable. In addition, this adjustment method is also used for position control. Both control algorithms contain disturbance correction loops that maintain the arm position regardless of external interference. This is particularly important in this study due to the high variability of the end effector in the dry box environment. Workers find themselves frequently manipulating objects and handling various tools, which results in varying amounts of force acting downward on the worker's arm. The control algorithms contain a correction algorithm which compensates for changes in position that do not originate from user input.

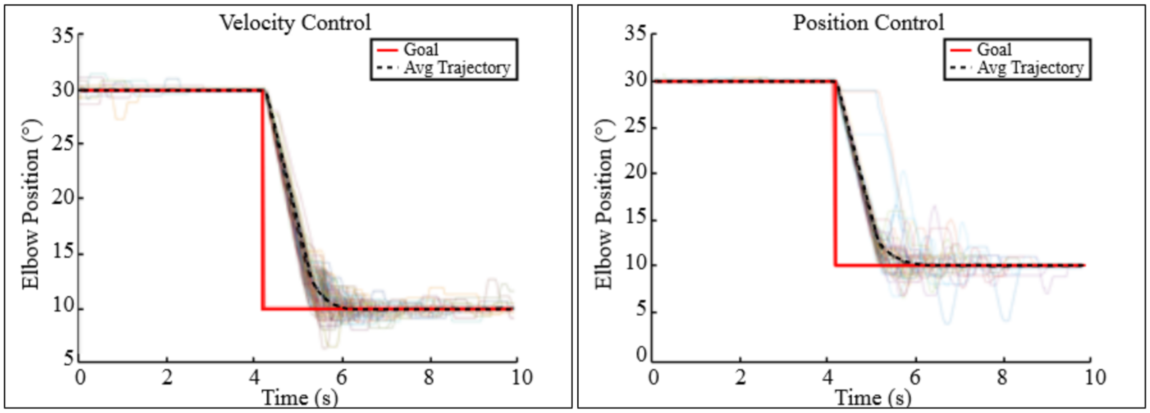

Figure 3.3: Position (left) and Velocity (right) control movement results. The red lines display the desired position change, and the black dotted line displays the average trajectory of the recorded movements. The individual trajectories are shown in various colors

3.3 Results

The sessions were compiled and analyzed in the MATLAB environment, and the control movement results can be seen in Fig. 3.3. The duration from initialized movement to final position attainment defined the speed of the system, and the user's ability to stabilize the exoskeleton in the predetermined angle measured the accuracy of the system. The final position was considered reached when the user finalized movement within 1% error of the total displacement amount. A t-test was performed to assess statistical significance between the performance of the two algorithms, which showed a significant difference with a p-value of 0.003. The average settling time for the position-based algorithm was of 2.02s, and the velocity algorithm performed at 3.04s. In terms of accuracy, the users were able to reach the desired positions within the 10 second time limit with 81% and 73% accuracy for the position control and velocity control, respectively. In addition, the average magnitude of error for each algorithm was of 1.25 degrees for the position algorithm, and of 2.10 degrees for the velocity algorithm.

3.4 Discussion

Two primary control algorithms were developed and tested, with unilateral performance improvement shown by the position-based algorithm. This position-based solution showed shorter settling times, which would allow for the user to quickly make changes to their position. The ability for the user to reach the desired position accurately displays that the user will be able to arrive at their desired position with little to no error, minimizing correction movements which would further hinder efficient work. Further, it is shown by the normalized error magnitude that the position algorithm has an overall smaller error when overshooting or undershooting the desired position. Further works will include a robust analysis of personalized parameter settings and the effect of these on the performance, as well as proportional and time-based control parameters to allow for a more dynamic range of movement options. The improvements in accuracy and settling time would improve the latency experienced by the user, resulting in a smoother, more ergonomic experience. In terms of neurorehabilitation, this control mechanism would provide sufficient assistance with consistent movement, meeting control requirements for acute rehabilitation.

The findings from this work motivated the following work due to the nuanced considerations required to stabilize the control system while obtaining the desired motion trajectories. For this reason, we further explore the operation margins of an advanced admittance controller which improves on this system by adding environmental awareness to the system in a dynamic way. The subsequent work aims to describe the design process of an admittance controller in the context of exoskeleton joint control by utilizing the intent detection methodologies explored in prior chapters and defining axioms of safe and stable control of such a device.

CHAPTER 4

ACCURATE TORQUE MODULATION IN REHABILITATION ROBOTICS USING ADMITTANCE CONTROL

4.1 Introduction

Reactive and adaptive robot control requires robust control awareness of the operation environment, and human-robot interactions are considered special cases within this environment [41]. Although operational safety is a primary focus of all control systems, the focus on safety in robotics meant for physical human interaction is especially important, as any unforeseen movement could cause severe injury to the user [42, 43, 44]. Further consideration must be taken in rehabilitation robotics due to the unstable physical conditions presented by neurorehabilitation patients [45, 46, 47]. As discussed previously, neurorehabilitation is a unique type of medical therapy required following injury to the nervous system. For maximum recovery, brain plasticity must be engaged, as it is the primary means of recovering neurological control [48, 49, 6, 50, 51, 52, 53, 54]. Recovery has been shown to be of maximal efficacy when it is performed shortly after the injury [5, 11, 12, 55]. Unfortunately, during the early stages of neurorehabilitation, patients tend to have a severe lack of muscular control and strength, as well as present with severe involuntary contractions during simple movements, referred to as spasticity [12, 55, 56, 57, 58, 59, 60]. Muscular compensation poses an additional challenge as it can cause long term dexterity impairment in patients. Admittance control serves as a strong foundation for rehabilitation robotics due to its robust response to simulating and manipulating the apparent dynamics of the system to achieve a desired system response. Traditional interaction-based control methods include - full-state interaction control [61, 62] indirect/direct force control [63], impedance control [64], and admittance control

[65, 66]. In this paper we discuss the composition of an admittance control system, usually used in haptic interaction controls. Using force measurements between the human and robot, the control system manipulates the set-point to a low-level controller through its virtual dynamics to get the desired response [67]. As the common controller used in this architecture is a velocity-following reference controller which conjugates force and velocity, we will use this as the assumed controller for the rest of the paper. Admittance control uses virtual dynamics which are consistent with kinetic and kinematic models [67, 68]. This allows a simulation of the system to be performed by adapting the relation between the velocity reference and the measured force triggering it. Admittance control can be considered a 2-layered impedance control, using the opposite of impedance to reflect a feedback layer of control, allowing for a more robust control of the apparent system dynamics[69, 70]. The ideal application for both impedance and admittance control are at opposing ends of the “haptic spectrum” [68, 70, 71, 72, 73, 74]. In admittance-controlled devices, it is easier to simulate stiff virtual surfaces and difficult to simulate low apparent inertia [42, 70, 75]. Impedance controlled devices, however, are more capable of simulating low inertia environments but are not ideal for simulating stiff virtual surfaces [70].

4.2 Motivation

Adaptive control has been used successfully in some rehabilitation robotic devices in the past [14, 76, 77, 19, 78, 18, 55, 79, 24, 80, 81]. Although there has been success with clinical deployment of several devices, specific limitations, properties, and operational stability margins are not universally applicable [65, 82, 83, 84, 85, 86]. Using passivity and stability, we can define margins for stable operation considering a coupled human user [43, 69, 87]. Assessing the apparent transfer function, we determine the adjustable variables which will limit the passivity of the system [88, 89] and supply the transfer function with average values based on the stability and passivity limitations established [90]. From that point, we then analyze the threshold of acceptable values for the coupled human in the closed-loop system [61, 90, 91]. The importance of margins of stability in rehabilitation devices stems from the unstable physical movements experienced by neurologically injured patients [5, 11, 12, 7, 92]. Patients undergoing neurorehabilitation not only need physical support and assistance to complete movements, but that assistance must also be aware that there is phenomenon like spasticity and compensatory contractions [6, 53]. Although these involuntary movements contribute to the force read by the sensor, they must not be considered in the control calculations and must be omitted from the output [69]. This is one of the primary challenges of early-stage rehabilitation, and the focus of the final analyses of the control schema. The coupled model is restricted to the same laws of mechanics, generalizing a second order polynomial transfer function to define the force based on the physical attributes of the coupled limb [85, 88]. When an able-bodied person is physically coupled to a robotic device, the range of values that represents the limb's mechanics is relatively narrow [85]. Neurorehabilitation patients experience spasticity, resulting in stiffened movements and restrictive contractions [12]. Under the same mechanical representation, the values reflecting the mechanics of the neurorehabilitation patients' limbs vary to a greater degree [70, 88, 93, 16]. Setting the broadest possible range of acceptable coupling values for the system will benefit control system tuning efforts. The system can be tuned with increased range while statistically guaranteeing the stability and safety of the system for a greater number of users [73, 87, 91]. We will analyze the effects of several subsystems of the admittance control system, including the use of feed-forward control, adding phase lead, torque signal filtering, a phase lead on motion reference, adding a complex gain, and how the addition of virtual damping on the system affects the performance, passivity, and stability when exploring minimal inertia admittance control. We also add a methodology for toggling passivity in the system during undesired scenarios such as muscular spasticity or compensatory contractions [12, 58]. Understanding, detecting, and adapting movements during therapy to dissuade improper motor learning is paramount, as a failure to recognize and correct these can lead to chronic impairment and long-term undesired effects in patients [12, 58, 60]. Concluding, these assessments lead to a set of recommendations and considerations to design a high-performance admittance control system with low apparent inertia and robust coupled stability. In the following analyses, a single degree of freedom (1-DOF), linear time invariant (LTI), single interface system with one-port admittance interaction is used.

4.3 Background

4.3.1 Admittance Control History and Origins

Admittance control originated in 1992 with the works of Newman, Gullapalli et. Al., Schimmels and Peshkin [65, 67, 94]. However, what is now referred to as admittance control can be found in literature as early as 1987 with Lawrence and Stoughton [84], referred to as ‘position-based’, ‘velocity-based impedance’, or even used interchangeably with ‘impedance’ control [68, 84, 95, 96, 97, 98, 99, 100, 101]. Although a difference can be noted that impedance control tracks motion whereas admittance control tracks force [41, 102], it is worth noting that admittance control can track both force and movement simultaneously. The desired motion characteristics which can be adjusted is referred to as the admittance, which is felt at the interaction point between the human and the robotic device. This behavior is referred to as driving point dynamics [103], mechanical drive point mobility [65], virtual dynamics [69, 70] desired dynamics [104], and target dynamics [44, 104].

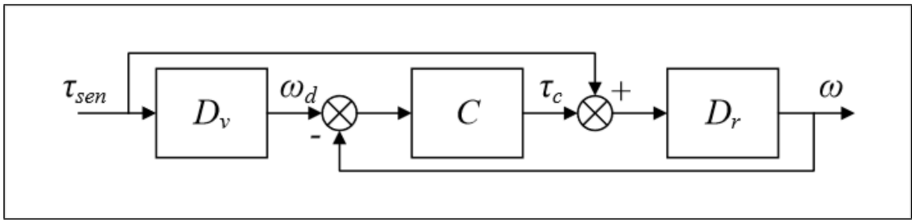

Figure 4.1: The basic admittance control diagram shown taking the torque input at the sensor τ_{sen} , setting a velocity reference point using the virtual dynamics ω_d, the error of which $(\omega_d - \omega)$ is then given to the controller (C) that outputs the desired torque which is then combined with the feed-forward element, finally processed by the robot dynamics (D_r) to output the velocity output

We will use the term virtual dynamics to refer to the desired behavior of the robotic arm and use these dynamics to modulate the reference value for the velocity controller. The dynamics experienced by the human are then subject to coupled close-loop behaviors which then contribute to and are referred to as the final *apparent dynamics*. Academic interest in interaction control ballooned after the works presented by [64] and [103] which focused on impedance control and passivity. Works by Hogan mention an impedance control like [66] which used indirect force control for industrial machinery control. Interaction-based control was first implemented for industrial applications like welding and deburring due to the high environmental friction and stiffness in the required machine motions [66, 94, 96, 102, 105]. Retrofitted industrial robots were equipped with accommodation and admittance control in [44, 63, 66, 98, 102, 106]. In the 1990s, [107] [108] mentioned devices with active control interacting safely with humans, and eventually led the development of admittance-based controlled robots such as [14, 76, 77, 19, 78, 18, 55, 79, 24, 80, 81].

4.3.2 Admittance Control Applications and Comparisons

Admittance and Impedance Control

Impedance control differs from admittance control in that impedance controls motion after a force is measured, whereas admittance controls the force after derivation from a setpoint is measured [69]. Impedance control is normally used in manual haptic and tele-operation devices [41]. Admittance control, however, is used most often in large non-backdriveable high friction devices which are usually wearable robotics or industrial machinery [72]. The primary reason to prefer an impedance control to admittance is that impedance controls forego the need for a force sensor, which can be expensive, sensitive to drift, and sensitive to environmental disturbances. Designing impedance controllers with open-loop force generation which perform adequately is relatively easy due to this. An undesired effect of such a controller is that the internal friction and other dynamics of the robot are still present in the apparent dynamics experienced [70]. This limitation leads to robotic designs that employ impedance control to also use lightweight (low inertia) and low friction (damping) setups to minimize the lingering disturbance. Explicit force feedback control can be used in admittance devices as shown in [70, 73, 104] which is shown to significantly reduce these apparent disturbances from the system dynamics. However, force feedback in low-frequency resonant modes and backlash will cause destabilization [70]. It is recommended to use closed-loop force feedback in impedance control and closed-loop velocity feedback in admittance controls.

Admittance Control in Neurorehabilitation

Control performance goals are based on the application. Knowing the link between impedance and admittance, we can now recognize the end goal of the control system

– to behave as the set dynamics describe. Admittance control enlists the use of an equation describing the mechanical characteristics of the desired movement [64, 107]. In this regard, the goal is subject to the mechanical equation. The system gets the force detected by the sensor and uses the virtual dynamics to calculate the reference velocity for the controller to follow [67, 109]. The addition of the closed coupled loop seen in Fig. 4.1 shows the way the kinetic feedback affects the controller. There is a feedback loop which reads the velocity output of the system and then determines how much of the recorded torque originates from the inherent kinetic properties of the human partner. When we look at neurorehabilitation and how pivotal it is for patients to initiate their therapy, we need to adjust the system to be as assistive and weightless as possible [49, 6, 110, 111]. To achieve this, two things must occur – we must set the proper admittance equation for internal kinetic elimination [67, 71], and we must have the system perform as close to the virtual dynamics as is possible [43, 109, 112]. The admittance feedback equation must adhere to the natural mechanics of the user's limb, and the virtual dynamics require the lowest possible inertia settings while maintaining stability [113, 114, 115]. We can then generalize the goal for admittance controls in neurorehabilitation robotics to be a two-pronged goal – provide weightless assistance and do so in a safe and stable manner. The following section will describe the methods used to define and determine stability across the individual and coupled systems.

4.4 Stability Criterion

Stability considerations for an interaction-based controller aims to fulfill several stability qualifications [103] –

- Independent stability – experienced when the environment does not contact the device
- Transitional Stability – experienced when the device transitions from free movement to coming into contact with the environment
- Coupled stability – experienced in a stable state of consistent interaction

Transitional stability is not relevant in a practical sense, as operation of rehabilitation robotics does not usually see the user decoupling with the device [116]. Decoupling mid-operation would be expected to occur in an industrial situation where the robotic device may be used for a portion of the task and transition from being manipulated to free movement. For this reason, we assume the device is in a stable stage of coupling, and the control is initiated when the device is either fully in contact or detached from the user.

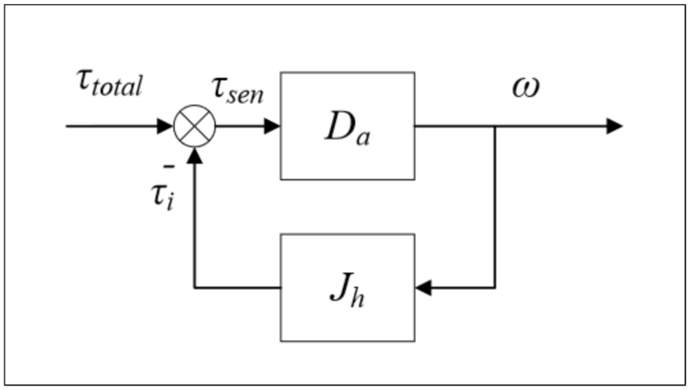

Figure 4.2: The full coupled admittance system with apparent dynamics $D_a(s)$ and human impedance $J_h(s)$. The total force measured τ_{total} is subtracted by the calculated human feedback torque τ_i to give the sensor torque τ_{sen} which is then processed by $D_a(s)$ to output ω

4.4.1 Coupled Stability

The exchange of power through forces experienced pivotally is shown as a coupled system in Fig. 4.2. This system is non-trivial as the two separate stable systems can show instability when coupled, and the unstable robot can become stable after coupling [103]. The apparent admittance $D_a(s)$ is shown coupled to the human impedance characteristics in $J_h(s)$, creating a force loop with negative feedback. The feedback causes the system's stability to be highly dependent on the user's limb characteristics [41]. This effect is crucially important, as the limb characteristics of neurorehabilitation patients exhibit a broader range of representative values than that of able-bodied workers using industrial wearable robotics.

4.4.2 Energy Passivity

Robust coupled stability can be attained by achieving energy passivity as denoted in [89]. The original term was used in electrical network coupling but has since then been used in human-robot interactions. A similar approach is used to guarantee stability of the system by defining the stability requirements of the final system when attached with an energetically passive couple. This can be easily achieved in controlled environments with predictable characteristics as can be found in industrial applications. However, human-robot interactions are special in that the user can exhibit active behaviors [117]. Due to our daily interactions with passive objects, we know that a human interfacing with energetically passive objects results in a stable interaction. Hence, we know if the robot's apparent dynamics are energetically passive, we have a stable system when it is coupled to the user. The remainder of this study will focus on attaining passivity of the apparent dynamics. Passivity, as well as good performance, are the primary design goals of such control systems, although we will only be studying the effects of passivity on the margins as will be discussed in section 4.4.3.

4.4.3 Passivity Criterion

In the work by Colgate [103] passivity for a one-port system is characterized by its inability to provide more energy than was put into it. This is exemplified by (4.1),

$$\int_{-\infty}^{t} \tau(\theta)\omega(\theta)\,d\theta \geq 0 \tag{4.1}$$

where the power-conjugated torque τ and angular velocity ω are the inputs and outputs of an impedance or admittance controller in a mechanical system. The designed controller must perform in accordance with (4.1) if the apparent dynamics are to embody the energy passivity that is desired. If the apparent dynamics are set properly and passivity is achieved, we can guarantee the coupled system will be stable under any coupling henceforth. Several conditions have been established to assess passivity of a control system in the frequency domain by Colgate [103] which apply to a 1-DOF, LTI-controlled robotic system, using ω_c to denote the angular frequency:

1. $D_a(s)$ has no poles in the complex plane.
2. $D_a(s)$ imaginary poles, if any, are simple with positive real residues.
3. $\Re\{D_a(j\omega_c)\} \geq 0, \forall\omega_c \in \mathbb{R}$ where the admittance is positive real for all positive and negative frequencies up to both Nyquist frequencies.

The first is a standard control stability condition which sets the uncoupled stability condition. The second and third conditions are called the positive real condition [103]. Simplifications for these conditions can be found in [44] to show that

$\Re\{\eta\}\Re\{\sigma\}+\Im\{\eta\}\Im\{\sigma\} \leq 0, \forall\omega_c \in \mathbb{R}$, where η and σ are the numerator and denominator of the apparent dynamics $D_a(j\omega)$ respectively, $\Re\{\eta\}$ is the real and $\Im\{\eta\}$ is the imaginary part of the numerator. With this setup, we have an even polynomial in angular frequency ω_c, for which we will look at the value for ω_c^0. If the value at ω_c^0 is zero, the remaining polynomial coefficients should be greater than or equal to zero, which satisfies the necessary passivity conditions when coupled with the uncoupled stability condition [118]. If the coefficient at ω_c^0 is non-zero, more steps must be taken. To conform to the passivity, we must find the marginal passivity conditions by using discriminant analysis for fourth order equations. Higher order equations do not have a clear generally applicable method. Generally straightforward equations demand that all coefficients be larger than zero for a polynomial in ω_c to guarantee a conservative passive system. The following passivity conditions performed in this work will take the more restrictive approach of requiring all coefficients to be greater than or equal to zero. When using this tactic, however, the pole-zero excess cannot exceed one in apparent dynamics $D_a(s)$, and the system has to be minimum phase, which requires no unstable zeroes. Arguments against enforcing passivity in human-robot interactions say that doing so is too restrictive to the system. As the practical margins of operation are bounded, a passivity requirement for an infinitely stiff (k_h), dissipative (β_h) or of infinite inertial mass (m_h) is too conservative for practical systems [70, 82, 90, 119, 120]. Using these broad conditions does not set the final values of operational stability, but provides significant information to understand the margins of possible combinations to ensure safety and stability no matter the characteristics of the human limb.

4.4.4 Coupled Z-width

Though we may wish to achieve passivity, it may not always be possible due to unwanted performance from the system, or even by other system limitations imposed by performance goals. When the apparent dynamics of the system are stable but not passive, [85] showed that stability can still be achieved by complementing the system parameterized in a quasi-linear matter to represent the dynamics in terms of inertia, stiffness, and damping [85, 107]. If we do not consider the inertial value, the application resembles z-width expressed in [121]. Since we can stabilize an active system by coupling it to an environment (or human limb) within a specific range of values, we can determine this range and call this the coupled z-width. We do this by testing the coupled system's stability while under a range of values for the mechanical characteristics of the human limb. This measure will determine the mechanical characteristics of the human limb, which are then coupled with the robotic system to make the apparent system marginally stable. This gamut value will provide the possible values of stiffness and damping that are stable if we were to exit strict passivity conditions, as previously discussed to be the preferred approach of some authors in the past. To evaluate the coupled z-width, we can evaluate the Huruwitz determinants or the Routh array for the closed loop coupled system with the transfer function shown in Fig. 4.2.

$$\frac{D_a(s)}{1 + D_a(s)J_h(s)} \tag{4.2}$$

Similarly, we can solve for the coupled z-width by calculating and assessing the Nyquist criterion of the open loop shown in $D_a(s)J_h(s)$. The coupled z-width calculated in this study was performed by studying the phase margins of $D_a(s)J_h(s)$

with a passive $J_h(s)$ in the form shown in (4.3),

$$\frac{1}{3}m_h l_h s + \beta_h + \frac{k_h}{s} \tag{4.3}$$

with m_h, l_h, β_h, and k_h representing the mass, radial length, dissipation (damping), and stiffness of the human limb, respectively, as illustrated in Fig. 4.3. Coupled z-width diagrams will show the range and mark the area of stable values. This technique, however, requires the mechanical characteristics of the human limb to be well described by (4.3). Whereas [107] shows this technique can be properly applied, [117] shows the technique was not adequate. It is because of this limitation that we can assume the diagram to show the theoretically valid values that promote stability, but the practical coupled z-width values will narrow the presented z-width values.

4.5 Controller Design

4.5.1 Physical simulation setup

As discussed previously, admittance control systems require several mathematical representations of the mechanical properties of several parts to accurately determine the desired and external kinetics and kinematics. The first equation to define is the mechanical representation of the arm, in terms of J_h. This equation was presented in section 4.4.4 and will be the same throughout the experiment. Similarly, we have a mechanical representation of the motor D_r, which encompasses the inertia I_r and damping β_r parameters, which are subject to manufacturer's specifications, along with the gearbox ratio k_g and the torque constant k_τ. Lastly, the virtual dynamics D_v of the system will be defined based on the movement characteristics desired. In this study, we will change the nature of the virtual dynamics, adding and changing

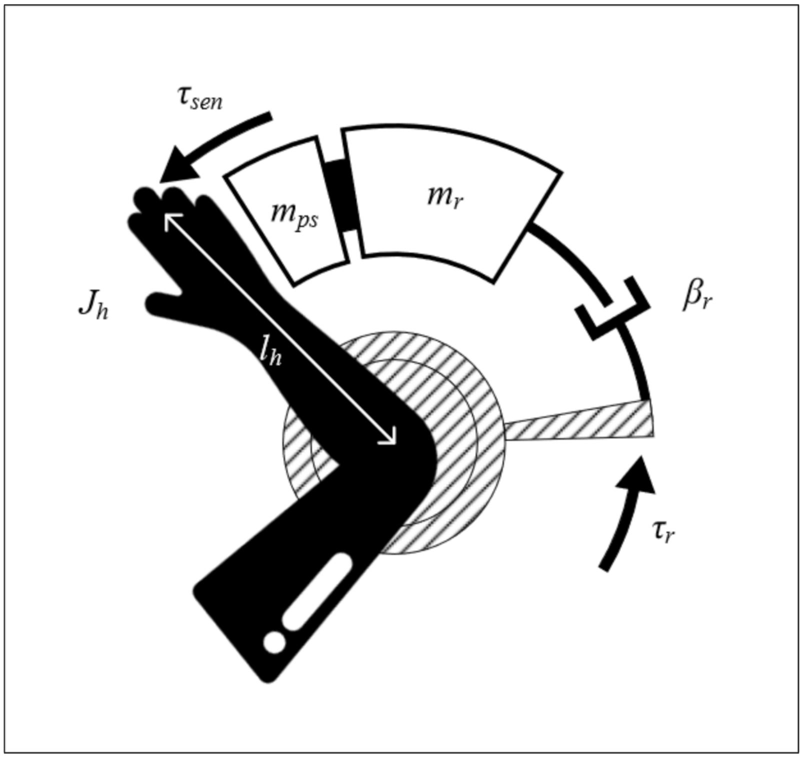

Figure 4.3: Physical Model setup. The human dynamics $J_h(s)$ when coupled with the system. The motor dynamics are in the form of an evenly distributed rod of mass m_r, rotating about one end length l_r, damping effect β_r, and post-sensor mass m_{ps}. The equation representing the arm $J_h(s)$ is represented by a similar mechanical equation consisting of m_h, l_h, and β_h, replacing m_r, l_r, and β_r, respectively

elements to evaluate the effect of those elements in improving the stability of the overall system. E_α, E_ω, and E_τ represent the observers for the acceleration, velocity and torque, respectively. The motor controller consists of the feedback-feed-forward loops (O_{fb}, O_{ff}) that feed into the current controller C_i, which follows the zero-order hold C_{zoh}. The full structure can be seen in Fig. 4.4.

4.5.2 Admittance control diagram

The apparent dynamics from D_a from Fig. 4.2 is expanded in Fig. 4.4 without the coupled J_h. Causality is shown when the force reading (τ_{sen}) is input, calcu-

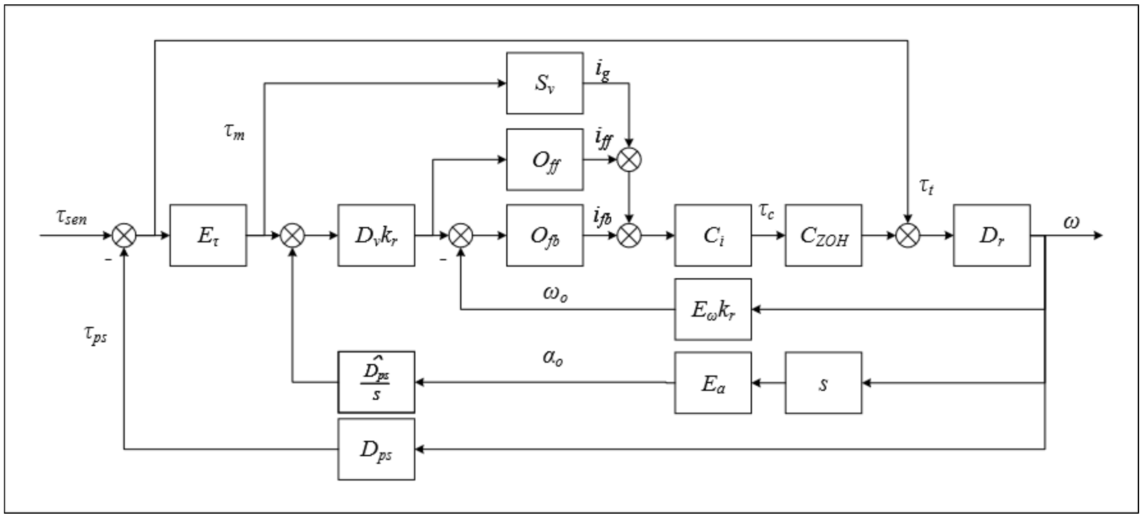

Figure 4.4: Fully expanded apparent dynamics D_a from Fig. 4.1 & 4.2. The total final transfer function can be found in appendix B. The defined symbols all are described in appendix A. The non-denoted sum junction (those without minus signs) are all summations

lating the signal to the movement in angular velocity (ω) as the system output. The transfer function to τ_{sen} to movement ω which shows the system's apparent dynamics is in appendix C. The control diagram subsections will be detailed here. All functions are dependent on the Laplace variable s. Naming methodology and symbol representation is contained in appendix A.

Torques experienced by the system

An externally applied torque (τ_{sen}) is applied on the system by the human limb. Torques from the post sensor dynamics act on the controller. The torques are measured by a force sensor with its operating bandwidth which is subject to observer dynamics (E_τ) and signal filtering.

Torque to angular velocity

The measured torques (τ_m) pass through the virtual dynamics ($D_v(s)$), which adapts the behavior to the desired values. A gear ratio k_g then multiplies the reference velocity of the virtual dynamics (ω_d) to the desired set-point. The resultant velocity is the controller's reference point.

Digital controller and resultant actuation

The controller outputs a desired electrical current to be used by the motor. The controller has a feed-forward and feedback controller (O_{ff},O_{fb}, respectively). The feedback controller is commonly of the proportional-integral (PI) type: $O_{fb} = k_p + \frac{k_i}{s}$. Additional force amplification gain (S_g) allows for apparent reduction in robot inertia and damping/friction effects. This gain element will consist of a 2nd order polynomial and allow for actuation clamping when spasticity and/or compensation are detected. The closed loop current controller (O') is presented with the current values calculated from the modulated gain, the feed-forward, and the feedback sections. From the controller calculation, the reading is held for a given sampling time (T_s) using a zero-order hold (ZOH). The controller is also assumed to have a high bandwidth as the expected industrial controllers often have more than 2 kHz, which along with some processing time, comprises the delays in the ZOH. The calculated current generates a torque in the motor (τ_c) that is acted on by the gear ratio, amplifying the reference torque value for the passive dynamics for the robot ($D_r(s)$).

Control output and impedance feedback

The total calculated torque is used to output the final robot motion. The motion is then observed by a velocity sensor or observer (E_ω) and an acceleration sensor or observer ($E_\alpha(s)$). The velocity reading is used in the internal velocity control loop, while the acceleration signal is used in compensation methods within ($\hat{D}_{ps}(s)$). Post sensor dynamics ($D_{ps}(s)$) are responsible for generating an impedance reaction torque (τ_{ps}) on the torque sensor, which then affects the robot dynamics $D_r(s)$ directly.

Control model

In order to generate a range of values to establish stability, a baseline model is constructed to study the coupled stability between the human limb and the robot device. The baseline model will be a robot model consisting of a rigid cylindrical rod rotating about an axis lined up with the robotic axis, as shown in Fig. 4.3. This model will be the reference point to compare results across the models tested in this study. The model will contain virtual dynamics and only feedback control as shown in Fig. 4.4 for the naïve admittance controller. The baseline system's apparent dynamics are displayed in $\overline{D_a}$. These dynamics are based on the robot being in contact with the human limb which applies torque τ_{sen}, which can be in the form of human impedance. The full model shown in Fig. 4.4 is then adapted to assume simplifications. The simplifications include using ideal velocity and torque observers/sensors ($E_\tau(s) = E_\omega(s) = 1$), the removal of the acceleration sensing loop ($E_\alpha(s) = 0$) and feed-forward controls ($S_g = O_{ff}(s) = 0$), and the assumption of a post sensor impedance of $D_{ps}(s) = \frac{1}{3} m_{ps} l_{ps}^3 s$. In order to add the effects of reflected inertia from the motor ($m_m k_g^2$) to the robot inertia (m_r'), we make the inertia $m_r = m_r' + m_m k_g^2$ and the damping $\beta_r = \beta_r' + \beta_m k_g^2$. The parameters used in the baseline model are presented in Table 4.1. The controller is tasked with making a 10kg inertia dampened robot feel like a pure inertia 2kg inertia arm. The system should behave in a way that the inertia is reduced by a 5 factor while the damping in the robot is removed altogether, allowing smooth low-effort movement. The equation for the system, shown in expanded form in appendix B, taking external torque detected in any form as $\tau_{sen}(t)$ is

$$(I_r + I_{ps})\dot{\omega}(t) + \beta_r \omega(t) = \tau_{sen}(t) + \tau_c(t) \tag{4.4}$$

in which I_r and β_r are the pre-sensor inertia and damping effect, whereas the I_{ps} refers to the post-sensor inertia of the system. The robot velocity is shown as $\omega(t)$, and $\tau_c(t)$ is the post-transmission torque applied by the motor. This equation can be Laplace transformed, and is shown in (4.5).

$$(I_r s + \beta_r)\omega(s) = \tau_{sen}(s) - I_{ps} s\omega(s) + \tau_c(s) \tag{4.5}$$

The following equations for this baseline model for virtual dynamics as described are shown in $(4.6 - 4.8)$ omitting the dependency on the s variable for legibility.

$$D_v(s) = \frac{1}{I_v s} \tag{4.6}$$

$$\omega_d = k_g D_v(\tau_{sen} - m_{ps}\omega s) \tag{4.7}$$

$$\tau_c = k_g \frac{k_p s + k_i}{s}(\omega_d - k_g v) \tag{4.8}$$

Where k_p and k_i are the controller proportional and integral coefficients, m_v and l_v are the mass and radius of the virtual dynamics, given by $D_v(s)$ in (4.6). The reference velocity (ω_d) calculation is provided by (4.7). Equation (4.8) shows the velocity controller in PI configuration which defines a controller force (τ_c) based on the velocity error ($e_v = \omega_d - k_g\omega$).

Initial stability determination

When all parameters are set as positive, the apparent dynamics created by $(4.5-4.8)$ has 3 poles – one pole at zero from the virtual dynamics and two stable complex poles from the PI controller. Defining these poles implies the individual stability for the robot when it is under free movement and is not coupled to the human limb. The apparent baseline admittance is shown in Fig. 4.5 as $D_a(s)$ which demonstrates the partial approach to the virtual dynamics $D_v(s)$. In low frequencies, post-sensor inertia cannot be removed by the naïve admittance controller due to the admittance modulus caused by an inertia offset from m_{ps}. To solve this problem, section 4.5.3 will show the proper approach. The apparent dynamics $\overline{D_a(s)}$ drop back to the robot dynamics $D_r(s)$ at high frequencies, introducing excess phase lag in the transition.

Uncoupled passivity

Robot passivity can only be certain if

$$I_v > 0$$

$$I_v \geq \frac{k_p k_g^2}{k_p k_g^2 + \beta_r} I_r \approx I_r \tag{4.9}$$

$$-\beta_r k_i k_g^2 \geq 0 \tag{4.10}$$

In (4.9) we form a passive equivalent system with the same inertia as the robot by defining the passivity limit by introducing a pole in $D_a(s)$ of higher frequency than that of the introduced zero. This causes passive inertia reduction to be impossible with a controller only feedback control with purely virtual inertia. Using (4.10), we can determine that we have to sacrifice low-frequency performance by making $k_i = 0$ since it cannot be made negative, as it would violate the uncoupled stability requirement. The sacrifice comes from the integral controller adding extra phase lag for low frequencies on top of the barely passive virtual inertia settings. Any amount of extra phase lag stemming from this activates the apparent admittance. In addition, having a large transmission ratio is also a destabilizing factor, as the effect is shown in (4.9). The passivity requirements conflict with both disturbance

Table 4.1: Parameter values for baseline system

Variable	Value
m_v	2 kg
l_v	0.4 m
k_g	1:1
m_r	10 kg
l_r	0.4 m
m_{ps}	2 kg
l_{ps}	0.4 m
β_v	5 Ns/m
k_p	100 Ns/m
k_i	2000 N/m

rejection and with overall performance as they require using a low transmission ratio as well as little to no integral gain.

Coupled stability

The system with parameters from Table 4.1 is not passive when uncoupled and will have a finite coupling parameter threshold for the human limb, as shown in Fig. 4.5. The lines on the coupled z-width graph show that there are cases for which the human arm can exhibit pure spring characteristics and still be under stable operation. The sharp slopes show that even a moderate increase in the damping parameter delivers a significant improvement to the stability margins of the other parameters. This coupled z-width will be the baseline for which we will compare other coupled z-widths in order to study the effects of these margins under different controller configurations.

Effects of Virtual Elements

As previously discussed, we can look at the naïve admittance controller to render pure virtual damping or pure virtual stiffness effects with little challenge. In order

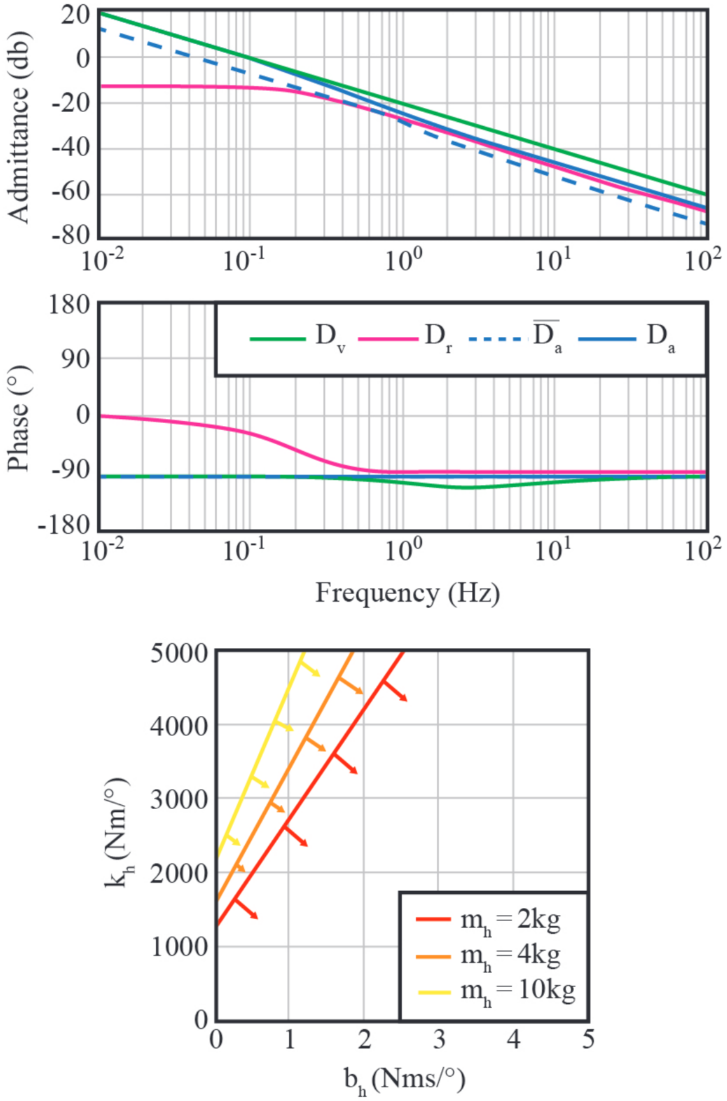

(b)

Figure 4.5: Bode response for the baseline system $D_a(s)$, with passive system $\overline{D_a(s)}$ shown in blue in (a), which shows that the passive system follows the linear response of the robot dynamics $D_r(s)$. The admittance and phase response for the robot dynamics $D_r(s)$ and virtual dynamics $D_v(s)$ are shown in pink and green plots, respectively. The coupled z-width is displayed in (b) with the lines and arrows defining the parameters which yield a stable coupled system. These values are based on the coupled baseline human system

to enable these virtual parameters, we will change the virtual dynamic equation to $D_v(s) = 1/\beta_v$ for accommodation form for pure damping. The passivity conditions become

$$\beta_v \geq 0$$

$$I_r K_i \leq (K_p + \beta_r)(K_p + \beta_v)$$

This shows that the K_i component should be kept low, and the virtual damping, the robotic damping, or the proportional gain k_p should be raised to meet the passivity conditions. The same tactic is applied for the purpose of giving the virtual dynamics a pure stiffness control in the shape of $D_v(s) = \frac{s}{k_v}$ and the passivity condition becomes the trivial $k_v \geq 0$ which is already a condition applied by the real positive condition discussed earlier. It is worth noting, however, that the two springs k_v and k_i are in series, shown by the apparent stiffness

$$k_a = \left(\lim s \to 0 \left(\frac{D_a}{s}\right)\right)^{-1} = \left(\frac{1}{k_v} + \frac{1}{K_i}\right)^{-1}$$

which also suffers from high influence from the gear ratio as it exponentially affects the K_i component. Combining these parameters yields the mass-spring-damper combination in the virtual dynamics. The final effect of these virtual dynamics can be seen in Table 4.2. The mass-damper combination is also discussed in the 4th design consideration below. Table 4.2 also shows the ranked results for each combination of parameters based on how these affect the coupled stability margins to gauge the importance of these configurations and their effects. Derivations to the passivity conditions are shown in appendix B.

4.5.3 Considerations for Optimization

It was shown in previous sections that the robot is capable of rendering passivity in combinations of pure stiffness and damping. We therefore focus on expanding the naïve model discussed in Fig. 4.4. We look at the newly coupled system and apply the same passivity criterion we applied earlier, we determine the z-width of the coupled system, and we determine the admittance tracking performance to assess the viability of the configurations as they are presented. In all cases, the baseline model discussed in 4.5 will be used and will always attempt to make a 10kg robot move like a 5kg after coupling. The following analysis will determine the effectiveness of these configurations and assess the improvement to the system as it is morphed.

Torque Signal Filtering

Using filtering on force and torque sensors is common practice as these sensors are often subject to disturbance from motion artifacts and electromagnetic noise, causing input noise and therefore output noise. If the virtual dynamics are purely inertia based and they do not account for the damping and stiffness parameters, filtering should be avoided. We can determine the phase lag introduced by filtering by considering $E_\tau(s) = B_n^{-1}(s)$ where the B_n is a Butterworth filter of n^{th} order, recognizing that an extra $\frac{n\pi}{2}$ rad phase lag is added to the apparent dynamics D_a for each order $n > 0$. Under the condition that $k_i = 0$, the time-constant low-pass filter would affect the passivity condition as shown in (4.11).

$$I_v \geq I_r * \frac{K_p}{K_p + \beta_r} + K_p T_\tau \tag{4.11}$$

Manipulating I_v to reach passivity will not decrease the inertia. Using a low-pass filter with $T_\tau > 0$ would worsen this effect as the virtual inertia I_v would need to increase to reach passivity. The effects on the coupled z-width are shown in Fig. 4.5(b) and display the reduced margins. The bode plot in Fig. 4.5(a) also shows that the device performs poorly in high frequency settings. Filtering, however, is sometimes inevitable such as for anti-aliasing, where the bandwidth should be as high as possible, and the filter order should be as low as possible.

Use Feed-forward Loop

Feed-forward control can be used when the controller is in torque or current control mode. It can be applied in form of a gain $S_v > 0$, or damping and inertia compen-

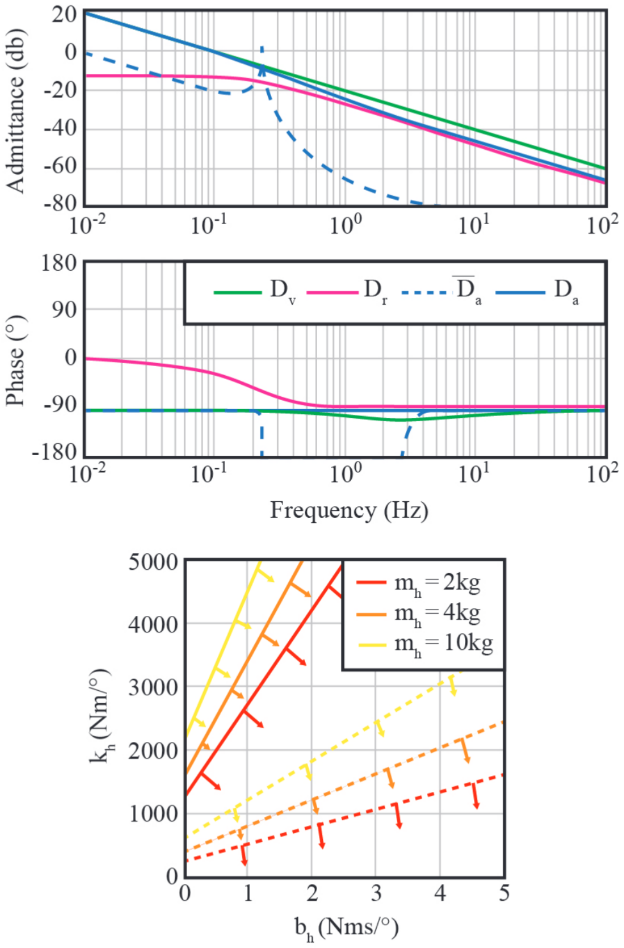

(b)

Figure 4.6: Attenuation, phase response, and coupled z-width of torque-filtered system ($T_\tau = 0.05$s) with baseline comparison. The coupled z-width is displayed in (b) with the filtered system in dashed lines for the same mass value, showing the narrowing of coupled z-width shown by the lower margins of stability

sation in the form of $O_{ff}(s) = \mu_{ff}s + \rho_{ff}$. Equations (4.12) and (4.13) then change to include the feed-forward control.

$$I_v \geq \frac{(K_p + \rho_{ff}k_g^2)I_r - (K_p + \beta_r)\mu_{ff}k_g^2}{(S_v k_g + 1)(K_p + \beta_r)} \tag{4.12}$$

$$0 \leq (\rho_{ff}k_g^2 - \beta_r)K_i \tag{4.13}$$

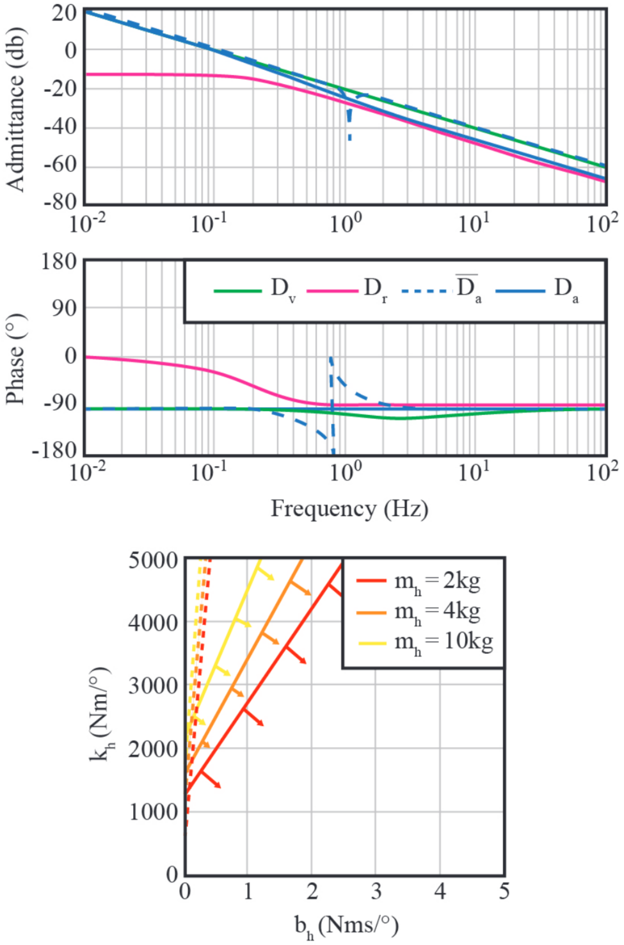

(b)

Figure 4.7: Attenuation, phase response, and coupled z-width of feed-forward-enabled system ($S_v = 0.05$, $\rho_{ff} = 2Nms/\deg$, $\mu_{ff} = 10\ Nm^2$) with baseline comparison. The coupled z-width is displayed in (b) with the feed-forward system in dashed lines for the same mass value, showing the significant widening of coupled z-width shown by the almost vertical dashed lines

By setting $\rho_{ff} k_g^2 \geq \beta_r$ in (4.13), we can get good low-frequency performance out of the apparent dynamics using the integral gain. The inertia from the robot is compensated by the inertial component μ_{ff} as there is subsequently less inertia to reduce from the feedback controller. Setting $S_v > 0$ removes the inertia that is introduced by the component ρ_{ff}. Due to the exponential effect of the transmission ratio, a high transmission ratio would reduce the passivity condition in (4.13) to

$$\mu_{ff} \geq \frac{k_p + \rho_{ff}}{k_p + \beta_m} I_m$$

showing that feed-forward is the only way to reduce inertia in high gear ratio controllers. Calculating the apparent inertia in high frequencies can be done by calculating $I_a = (\lim_{s \to \infty} (sD_a))^{-1}$ which results in

$$I_a = I_{ps} + \frac{I_r}{\frac{\mu_{ff}}{I_v} k_g^2 + S_v k_g + 1}.$$

This apparent inertia shows that with feed-forward components μ_{ff} and S_v set to zero, the apparent inertia of the system is both the post-sensor inertia I_{ps} and the robot inertia I_r, which adheres to the system characteristics shown in Fig. 4.7.

Virtual Damping

Pure inertial admittance equations can be changed to include a small amount of damping in most cases. The damping is not noticeable in small amounts, but would contribute to stability in low frequencies due to the phase lead it introduces. This lead can be useful as it counteracts the phase lag introduced by controller bandwidth or long system delays. Adding virtual damping in the form of $D_v(s) = \frac{1}{I_v s + \beta_v}$ results in a passivity condition of

$$K_i \leq \beta_v \frac{(K_p + \beta_v)(K_p + \beta_r)}{\beta_r I_v + \beta_v I_r}$$

Since the passivity condition found in (4.9) does not change, we know it cannot lower the virtual inertia of the system. Low frequency tracking is improved with virtual damping as can be seen in Fig. 4.8.

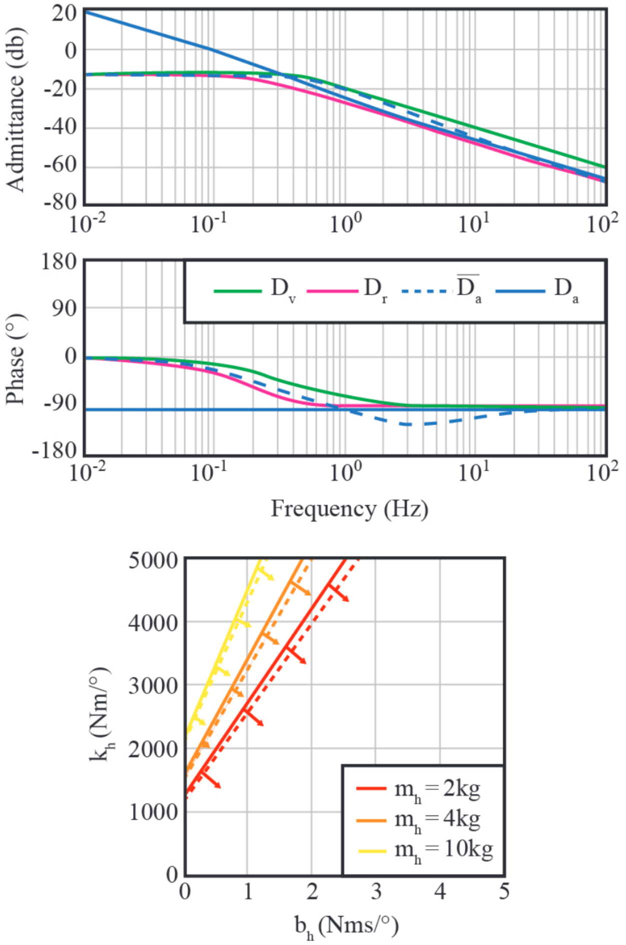

(b)

Figure 4.8: Attenuation, phase response, and coupled z-width of system with virtual damping enabled ($\beta_v = 3$ Nms/deg), and baseline comparison. The coupled z-width is displayed in (b) with the tested system in dashed lines for the same mass value, showing a minimal broadening of coupled z-width shown by the almost vertical dashed lines

Modification of angular velocity reference

The use of admittance controllers on retrofitted industrial controllers is common when the original proportional-integral/proportional-derivative (PI/PD) controller is what is referred to as a black box. When this is the case and we cannot manipulate the controller feedback/feed-forward parameters, we must look elsewhere to improve

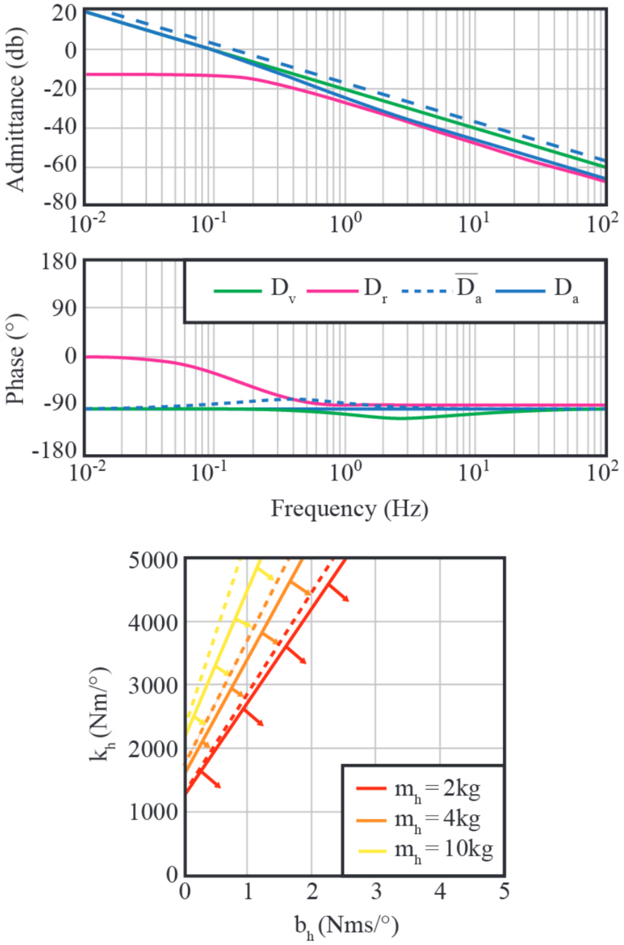

(b)

Figure 4.9: Attenuation, phase response, and coupled z-width of system with velocity modulated ($k_\alpha = 1$), and baseline comparison. The coupled z-width is displayed in (b) with the tested system in dashed lines for the same mass value, showing a minimal narrowing of coupled z-width shown by the almost vertical dashed lines

admittance accuracy and maintain broad coupled z-width. Adding an acceleration feed-forward to D_v with gain k_α would result in $D_v = (sk_\alpha + 1)D_v^*$ where D_v^* is the intended virtual dynamics of the system. Doing this would improve the high frequency tracking due to the phase lead introduced. The passivity conditions then become

$$I_v \geq \frac{K_p I_r - k_\alpha(K_p^2 + K_p\beta_r - K_i I_r)}{K_p + \beta_r}$$
$$0 \leq K_i(k_\alpha K_i - \beta_r)$$

which lets us know we would ideally want a robot with low inertia and we would need a low inertial gain k_i to see the benefits of the acceleration feed-forward. While the attenuation and phase responses show that the apparent dynamics adhere better to the virtual dynamics desired, the coupled z-width results show that the use of this acceleration feed-forward component provides marginal improvement.

Velocity controller bandwidth

The use of a low k_p and k_i are required for most of the passivity conditions derived from previous recommended configurations. We are often limited by controller characteristics but this can be minimized by increasing the bandwidth of the controller which pushes phase lag to higher frequencies. This effect drastically increases the coupled z-width as the effects of phase lag become observable only in instances of extremely high stiffness values of the coupled system. The subsequent effect of this is the considerable broadening of the coupled z-width while allowing for more broad settings of the controller gains k_p and k_i, which in turn allow for more disturbance rejection and suppression of parasitic dynamics. We can achieve this by offsetting time delays caused by the phase lag of the system, which is caused by the zero-order hold components in $C_{zoh}(s)$. The dynamics for such a ZOH are given by $C_{zoh}(s) = \frac{1-e^{-sT_s}}{sT_s}$ which intrinsically performs with a -90° at $\omega_{Nyq} = \frac{\pi}{T_s}$, with

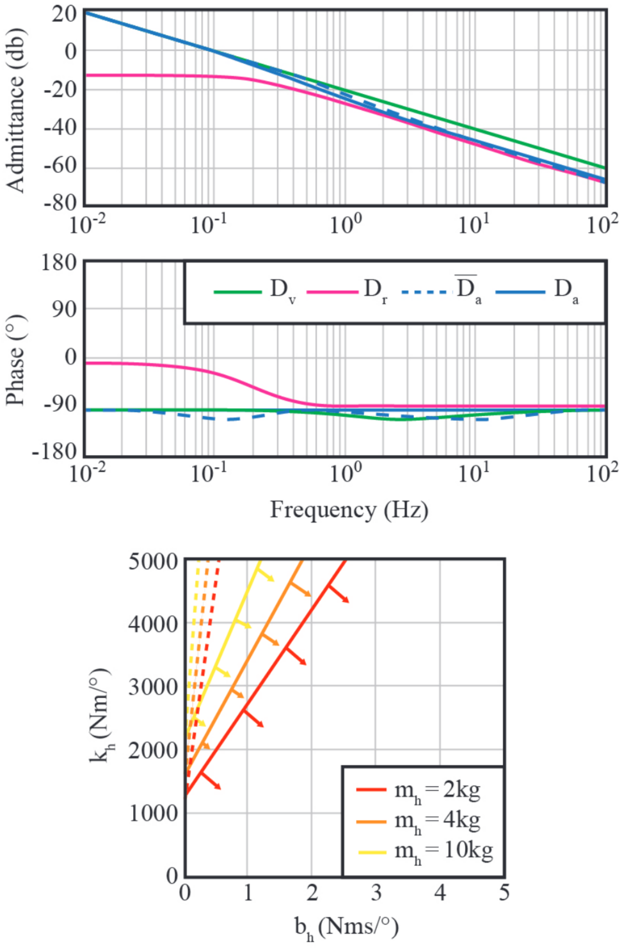

(b)

Figure 4.10: Attenuation phase response, and coupled z-width of system with velocity bandwidth enhanced ($k_d = 25\ Ns^2m/$ deg, $\tau_d = 0.1s$), and baseline comparison. The coupled z-width is displayed in (b) with the tested system in dashed lines for the same mass value, showing a minimal narrowing of coupled z-width shown by the almost vertical dashed lines

ω_{Nyq} as the Nyquist frequency. With an initial phase lag of -90° at $\omega\ T_s = \frac{\pi}{2}$, we remove any form of pure delay from the system. If we wish to optimize the system further, we can tune T_s down until the phase lag is compensated properly. Additionally, we can add a differential portion to the internal controller feedback. Adding this element changes $O_{fb} = k_p + \frac{k_i}{s} + \frac{k_d s}{T_d s+1}$ where k_d is the differential gain, and T_d is a low-pass filter time constant. Revisiting the passivity conditions for the following section yields the condition for passivity changed for (4.12) but not for (4.13). The new condition becomes $I_v \geq \frac{K_p I_r + \beta_r K_i T_d^2 - \beta_r K_d}{K_p + \beta_r}$ where $K_d = k_g^2 k_d$ which shows that the virtual inertia must be increased if $K_i \geq 0$ and $T_d \geq 0$. Using this technique alone, however, will not improve the passivity of the system if these two values are not zero. The controller behaves as expected, where the lower frequencies yield apparent dynamics closely resembling that of the virtual dynamics, and then approaches the robot dynamics as the frequency increases.

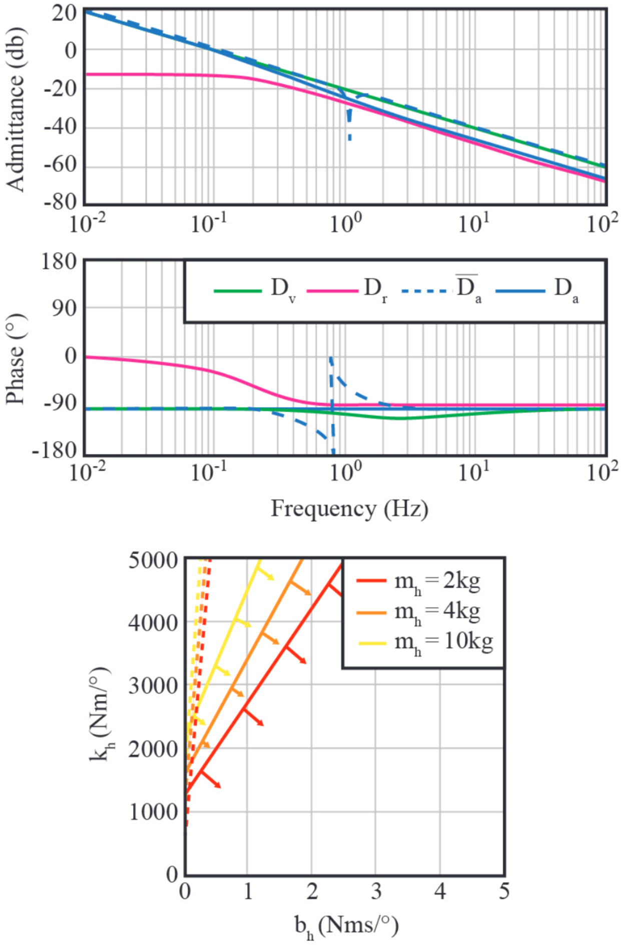

(b)

Figure 4.11: Attenuation, phase response, and coupled z-width of complex gain enabled system ($\mu_{sv} = 5$, $\beta_{sv} = 2$, $\rho_{ff} = 2Nms/\deg$, $\mu_{ff} = 10\ Nm^2$) It can be seen that the response is almost identical to the consideration in the feed-forward section

Table 4.2:

Rank	Consideration	Benefit	Constraints
1	Include feed-forward control	Minimizes the effective robot inertia which is then removed by the admittance loop	$\mu_{ff} < m_v$ $\rho_{ff} k_r^2 \geq 0$
2	Velocity controller bandwidth	Improves phase lag by pushing it to higher frequencies, effectively removing the lag under expected operation	$k_i \leq 0$
3	Virtual damping	Significantly improves control in low frequencies, but only moderately affects stability	$K_i \beta_v \geq 0$
4	Modification of angular velocity reference	Can introduce a phase lead, but restricts the coupled stability values	$k_i \neq 0$ $T_d \neq 0$ $k_a \geq 0$
5	Use Complex Gain	Additional complex gain can help fine tune offsetting the undesired inertia from the feed-forward gains	$\mu_{ff} < m_v$ $\rho_{ff} k_r^2 \geq 0$
6	Input Torque Signal Smoothing	Input signal filtering should be avoided as much as possible to avoid introducing phase lag to the system	T_τ as low as possible Filter order n as low as possible

Use Complex Gain Loop

We discussed the benefits of introducing a feed-forward component which included a static gain component in the form of S_v, and how this component helped mitigate the inertia imposed by the feed-forward equation $C_{ff}(s) = \mu_{ff}s + \beta_{ff}$. In order to have a more detailed control of apparent inertia manipulation, we can inject the complex gain in the form of $S_v(s) = \mu_{sv}s + \beta_{sv}$. It is just as relevant to pinpoint elements to improve stability as it is to identify additional sub-components, which can be employed to tailor the system behaviors while leaving the stability unaffected. As found in the feed-forward consideration, the apparent inertia defaults to the post-sensor inertia I_{ps}. This implies that the minimum performance capability of the system is not deteriorated, and the system response can be seen in Fig. 4.11.

4.5.4 Discussion

Admittance controllers provide a robust controller schema providing widely adaptive and beneficial awareness to the controller, therefore elevating the system's operating capabilities based on the robot's ability to interact with a broad range of objects and subjects. With interaction as the main concern of admittance controllers, we sought to maximize the system's coherence to the desired virtual dynamics. Using a baseline system with feedback provides a stable platform on which to design and develop a functioning controller, however when the system is coupled to another object as is necessary in neurorehabilitation, the system can experience instability. To account for the weak muscular strength and control in neurorehabilitation patients, when we design a controller for such a task, we wish to set the apparent dynamics of the system as low in inertia as possible, resulting in relatively weightless apparent dynamics. Understanding that independently stable systems can come to form an unstable system when they are coupled, this work has presented several design considerations to properly assert how enabling and changing different sub-components within the control system changes the gamut of parameters which result in a stable coupled system. The results, shown in Table 4.2, show the effects of each of these examinations and lists them in order of magnitude of benefit to the stability of the coupled system. Using the margins of improvement in the coupled Z-widths of the proposed systems, we can define the highest improvement gained from including feed-forward in the system. The effective inertia the dynamics have to cancel out are lower, thus giving better adherence to the virtual dynamics while significantly improving the margins of stability. Considerations to improve the sensor bandwidth will also improve the control as long as the integral gain k_i is less than zero, which violates the passive real condition. In actuality, this does not mean the system would cease to be stable, as coupled stability is not inherited from independent stability. A control designer can destabilize the coupled system easily by over-filtering the input signal, which in this case is the torque. Using these guiding principles, a neurorehabilitation therapy device would function in a safe and intended manner for a broad range of patients with unique physiological effects from their neural injuries.

4.5.5 Conclusion

Throughout this document, we have undertaken and addressed some of the considerations one must take when striving to develop an exoskeleton device for neurorehabilitation. The goal of the study was two-fold. The first goal was to assess those considerations and implement them in the development of an exoskeleton device that can potentially assist early-stage neurorehabilitation patients. The second goal was to design and optimize a control algorithm that would best assist those patients, who present with little to no muscular toning and require maximum assistance, while also maximizing neural involvement. We initially set out to build and develop an exoskeleton device for worker use with support from the DOE. We defined mechanical design considerations to establish a safe, lightweight, and comfortable device. By testing various algorithms and assessing device stability in the face of a variable environment, including specific temperature and space considerations, this device was then used for testing different control mechanisms to establish accurate and stable control. This process helped clarify mechanical considerations and also helped us develop an exoskeleton device that was indeed lightweight, comfortable, and met the needs of acute neurorehabilitation devices. Following, a variety of marginal analyses were conducted on an admittance control structure while establishing the operating values required for stable coupled operation between a human and robot exoskeleton. We determined that using a feed-forward loop would provide the highest coupled stability and is therefore most recommended, as opposed to signal smoothing which should be avoided unless strictly required because the resultant stability margins are narrowed significantly. Through these explorations, we have defined various key elements which are in dire need of standardization, and we hope to have provided sufficient analyses and effort in that direction.

Future Direction

The design and development of exoskeleton-type devices demands a comprehensive understanding of mechanical and control design, signal collection and processing, materials considerations, and interfacing, among a myriad others. Full development of such devices can see the device undergoing significant changes throughout development as new technologies and implementations become available. For example, limitations would significantly change if EMG electrode technologies allowed for continuous fine motor signal collection. Continuation of this work would entail the development of more refined control methodologies, further optimizing the admittance controller to account for disturbance estimation and utilizing a Kalman filter for trajectory smoothing. In addition, further work will require a multiple-joint implementation, which will then require inverse and reverse kinematics to calculate synergistic angular displacement.

BIBLIOGRAPHY

[1] C. for Disease Control and Prevention, "Stroke facts, https://www.cdc.gov/stroke/facts.html," 2022.

[2] L. M. Julius, J. S. Brach, D. M. Wert, and J. M. VanSwearingen, "Perceived effort of walking: Relationship with gait, physical function and activity, fear of falling, and confidence in walking in older adults with mobility limitations," *Physical Therapy*, vol. 92, pp. 1268–1277, 2012.

[3] A. Schinkel-Ivy, E. L. Inness, and A. Mansfield, "Relationships between fear of falling, balance confidence, and control of balance, gait, and reactive stepping in individuals with sub-acute stroke," *Gait and Posture*, vol. 43, pp. 154–159, 2016.

[4] B. Dobkin, H. Barbeau, D. Deforge, J. Ditunno, R. Elashoff, D. Apple, M. Basso, A. Behrman, L. Fugate, and S. Harkema, "The evolution of walking-related outcomes over the first 12 weeks of rehabilitation for incomplete traumatic spinal cord injury: the multicenter randomized spinal cord injury locomotor trial," *Neurorehabilitation and neural repair*, vol. 21, pp. 25–35, 2007.

[5] L. H. Schwamm, "What you need to know about strokes.," *National Institute of Neurological Disorders and Stroke*, vol. 4, pp. 1–6, 2004.

[6] B. B. Johansson, "Current trends in stroke rehabilitation. a review with focus on brain plasticity," *Acta Neurologica Scandinavica*, vol. 123, pp. 147–159, 2011.

[7] N. S. Ward, M. M. Brown, A. J. Thompson, and R. S. Frackowiak, "Neural correlates of motor recovery after stroke: A longitudinal fmri study," *Brain*, vol. 126, pp. 2476–2496, 2003.

[8] T. Proietti, V. Crocher, A. Roby-Brami, and N. Jarrasse, "Upper-limb robotic exoskeletons for neurorehabilitation: a review on control strategies," *IEEE reviews in biomedical engineering*, vol. 9, pp. 4–14, 2016.

[9] J. C. Perry, J. Rosen, and S. Burns, "Upper-limb powered exoskeleton design," vol. 12, pp. 408–417, 2007.

[10] W.-S. Ryu, K.-S. Hong, S.-W. Jeong, J. E. Park, B. J. Kim, J.-T. Kim, K. B. Lee, T. H. Park, S.-S. Park, J.-M. Park, *et al.*, "Association of ischemic stroke

onset time with presenting severity, acute progression, and long-term outcome: A cohort study," *PLoS medicine*, vol. 19, no. 2, p. e1003910, 2022.

[11] S. Demain, R. Wiles, L. Roberts, and K. McPherson, "Recovery plateau following stroke: Fact or fiction?," *Disability and Rehabilitation*, vol. 28, pp. 815–821, 2006.

[12] K. Honaga, Y. Masakado, T. Oki, Y. Hirabara, T. Fujiwara, T. Ota, A. Kimura, and M. Liu, "Associated reaction and spasticity among patients with stroke," *American Journal of Physical Medicine and Rehabilitation*, vol. 86, pp. 656–661, 2007.

[13] G. Monardo, C. Pavese, I. Giorgi, M. Godi, and R. Colombo, "Evaluation of patient motivation and satisfaction during technology-assisted rehabilitation: an experiential review," *Games for health journal*, vol. 10, no. 1, pp. 13–27, 2021.

[14] H. M. Qassim and W. Z. W. Hasan, "A review on upper limb rehabilitation robots," 10 2020.

[15] R. Bogue, "Exoskeletons and robotic prosthetics: A review of recent developments," *Industrial Robot*, vol. 36, pp. 421–427, 2009.

[16] F. Domrös, D. Störkle, J. Ilmberger, and B. Kuhlenkötter, "Converging clinical and engineering research on neurorehabilitation," *Converging Clinical and Engineering Research on Neurorehabilitation*, vol. 1, pp. 409–413, 2013.

[17] B. Chen, B. Zi, Z. Wang, L. Qin, and W. H. Liao, "Knee exoskeletons for gait rehabilitation and human performance augmentation: A state-of-the-art," *Mechanism and Machine Theory*, vol. 134, pp. 499–511, 2019.

[18] H. I. Krebs, M. Ferraro, S. P. Buerger, M. J. Newbery, A. Makiyama, M. Sandmann, D. Lynch, B. T. Volpe, and N. Hogan, "Rehabilitation robotics: pilot trial of a spatial extension for mit-manus," *Journal of neuroengineering and rehabilitation*, vol. 1, pp. 1–15, 2004.

[19] J. L. Pons, E. Rocon, R. Ceres, D. Reynaerts, B. Saro, S. Levin, and W. V. Moorleghem, "The manus-hand dextrous robotics upper limb prosthesis: mechanical and manipulation aspects," *Autonomous Robots*, vol. 16, pp. 143–163, 2004.

[20] N. Hogan, H. Krebs, J. Charnnarong, P. Srikrishna, and A. Sharon, "Mit-manus: a workstation for manual therapy and training. i," pp. 161–165, 1992.

[21] N. S. Seyfi and A. K. Khalaji, "Robust lyapunov-based motion control of a redundant upper limb cable-driven rehabilitation robot," *Robotica*, pp. 1–23, 2022.

[22] M. Bernhardt, M. Frey, G. Colombo, and R. Riener, "Hybrid force-position control yields cooperative behaviour of the rehabilitation robot lokomat," pp. 536–539, 2005.

[23] F. Baronchelli, C. Zucchella, M. Serrao, D. Intiso, and M. Bartolo, "The effect of robotic assisted gait training with lokomat® on balance control after stroke: systematic review and meta-analysis," *Frontiers in Neurology*, vol. 12, p. 1073, 2021.

[24] T. Nef, M. Mihelj, and R. Riener, "Armin: A robot for patient-cooperative arm therapy," *Medical and Biological Engineering and Computing*, vol. 45, pp. 887–900, 2007.

[25] S. Kotov, V. Y. Lijdvoy, A. Sekirin, K. Petrushanskaya, and E. Pismennaya, "The efficacy of the exoskeleton exoatlet to restore walking in patients with multiple sclerosis," *Zhurnal nevrologii i psikhiatrii imeni SS Korsakova*, vol. 117, no. 10. Vyp. 2, pp. 41–47, 2017.

[26] P. Cordo, H. Lutsep, L. Cordo, W. G. Wright, T. Cacciatore, and R. Skoss, "Assisted movement with enhanced sensation (ames): coupling motor and sensory to remediate motor deficits in chronic stroke patients," *Neurorehabilitation and neural repair*, vol. 23, no. 1, pp. 67–77, 2009.

[27] C. Tefertiller, B. Pharo, N. Evans, and P. Winchester, "Efficacy of rehabilitation robotics for walking training in neurological disorders: a review.," *Journal of Rehabilitation Research & Development*, vol. 48, no. 4, 2011.

[28] H. I. Krebs, J. J. Palazzolo, L. Dipietro, M. Ferraro, J. Krol, K. Rannekleiv, B. T. Volpe, and N. Hogan, "Rehabilitation robotics: Performance-based progressive robot-assisted therapy," *Autonomous robots*, vol. 15, no. 1, pp. 7–20, 2003.

[29] P. K. Artemiadis and K. J. Kyriakopoulos, "Emg-based position and force estimates in coupled human-robot systems: Towards emg-controlled exoskeletons," *Experimental Robotics*, pp. 241–250, 2009.

[30] R. A. R. C. Gopura, K. Kiguchi, and Y. Li, "Sueful-7: A 7dof upper-limb exoskeleton robot with muscle-model-oriented emg-based control," *2009 IEEE/RSJ International Conference on Intelligent Robots and Systems*, pp. 1126–1131, 2009.

[31] T. Lenzi, S. M. M. D. Rossi, N. Vitiello, and M. C. Carrozza, "Intention-based emg control for powered exoskeletons," *IEEE transactions on biomedical engineering*, vol. 59, pp. 2180–2190, 2012.

[32] J. Rosen, M. Brand, M. B. Fuchs, and M. Arcan, "A myosignal-based powered exoskeleton system," *IEEE Transactions on systems, Man, and Cybernetics-part A: Systems and humans*, vol. 31, pp. 210–222, 2001.

[33] Y. M. Aung and A. Al-Jumaily, "Estimation of upper limb joint angle using surface emg signal," *International Journal of Advanced Robotic Systems*, vol. 10, p. 369, 2013.

[34] R. Gopura, K. Kiguchi, and E. Horikawa, "A study on human upper-limb muscles activities during daily upper-limb motions," *International Journal of Bioelectromagnetism*, vol. 12, pp. 54–61, 2010.

[35] T. K. K. Koo and A. F. T. Mak, "Feasibility of using emg driven neuromusculoskeletal model for prediction of dynamic movement of the elbow," *Journal of electromyography and kinesiology*, vol. 15, pp. 12–26, 2005.

[36] E. P. Doheny, M. M. Lowery, D. P. FitzPatrick, and M. J. O'Malley, "Effect of elbow joint angle on force–emg relationships in human elbow flexor and extensor muscles," *Journal of Electromyography and Kinesiology*, vol. 18, pp. 760–770, 2008.

[37] O. Bai, R. Ramon, S. S. Divvela, E. Engeberg, and L. Lagos, "Worker fatigue measurement during prolonged nuclear facility operation," *2nd IFAC Conference on Cyber-Physical and Human Systems 2018*, 2018.

[38] R. Bogue, "Exoskeletons – a review of industrial applications," vol. 5, pp. 585–590, 2018.

[39] A. Herrel, V. Schaerlaeken, C. Ross, J. Meyers, K. Nishikawa, V. Abdala, A. Manzano, and P. Aerts, "Electromyography and the evolution of motor control: Limitations and insights," *Integrative and Comparative Biology*, vol. 48, pp. 261–271, 2008.

[40] R. Jimenez-Fabian and O. Verlinden, “Review of control algorithms for robotic ankle systems in lower-limb orthoses, prostheses, and exoskeletons,” *Medical engineering physics*, vol. 34, pp. 397–408, 2012.

[41] G. Zeng and A. Hemami, “An overview of robot force control,” *Robotica*, vol. 15, pp. 473–482, 1997.

[42] W. S. Newman and Y. Zhang, “Stable interaction control and coulomb friction compensation using natural admittance control,” *Journal of robotic systems*, vol. 11, pp. 3–11, 1994.

[43] W. Yu, R. C. Rodriguez, and X. Li, “Neural pid admittance control of a robot,” *2013 American Control Conference*, pp. 4963–4968, 2013.

[44] M. Dohring and W. Newman, “The passivity of natural admittance control implementations,” *2003 IEEE International Conference on Robotics and Automation (Cat. No. 03CH37422)*, vol. 3, pp. 3710–3715, 2003.

[45] L. Marchal-Crespo and D. J. Reinkensmeyer, “Review of control strategies for robotic movement training after neurologic injury,” *Journal of NeuroEngineering and Rehabilitation*, vol. 6, 2009.

[46] K. I. M. D. Anderson, “Targeting recovery,” *Journal of Neurotrauma*, vol. 21, pp. 1371–1383, 2004.

[47] P. Beckerle, G. Salvietti, R. Unal, D. Prattichizzo, S. Rossi, C. Castellini, S. Hirche, S. Endo, H. B. Amor, M. Ciocarlie, F. Mastrogiovanni, B. D. Argall, and M. Bianchi, “A human-robot interaction perspective on assistive and rehabilitation robotics,” *Frontiers in Neurorobotics*, vol. 11, pp. 1–6, 2017.

[48] B. A., A. F., N. S.M., B. J.H., P. G.B., and S. A.H.A., “Training modalities in robot-mediated upper limb rehabilitation in stroke: A framework for classification based on a systematic review,” *Journal of NeuroEngineering and Rehabilitation*, vol. 11, pp. 1–15, 2014.

[49] J.-M. Belda-Lois, S. M. del Horno, I. Bermejo-bosch, J. C. Moreno, J. L. Pons, D. Farina, M. Iosa, M. Molinari, F. Tamburella, A. Ramos, A. Caria, T. Solis-escalante, C. Brunner, and M. Rea, “Rehabilitation of gait after stroke:a top down approach,” *Journal of NeuroEngineering and Rehabilitation*, vol. 66, 2011.

[50] S. E. Fasoli, H. I. Krebs, M. Ferraro, N. Hogan, and B. T. Volpe, "Does shorter rehabilitation limit potential recovery poststroke?," *Neurorehabilitation and Neural Repair*, vol. 18, pp. 88–94, 2004.

[51] E. Guglielmelli, M. J. Johnson, and T. Shibata, "Guest editorial: Special issue on rehabilitation robotics," *IEEE Transactions on Robotics*, vol. 25, pp. 477–480, 2009.

[52] A. Koenig, X. Omlin, D. Novak, and R. Riener, "A review on bio-cooperative control in gait rehabilitation," *IEEE International Conference on Rehabilitation Robotics*, 2011.

[53] R. Colombo, F. Pisano, S. Micera, A. Mazzone, C. Delconte, M. C. Carrozza, P. Dario, and G. Minuco, "Robotic techniques for upper limb evaluation and rehabilitation of stroke patients," *IEEE transactions on neural systems and rehabilitation engineering*, vol. 13, pp. 311–324, 2005.

[54] P. Heo, G. M. Gu, S. jin Lee, K. Rhee, and J. Kim, "Current hand exoskeleton technologies for rehabilitation and assistive engineering," *International Journal of Precision Engineering and Manufacturing*, vol. 13, pp. 807–824, 2012.

[55] O. Lennon, M. Tonellato, A. D. Felice, R. D. Marco, C. Fingleton, A. Korik, E. Guanziroli, F. Molteni, C. Guger, R. Otner, and D. Coyle, "A systematic review establishing the current state-of-the-art, the limitations, and the desired checklist in studies of direct neural interfacing with robotic gait devices in stroke rehabilitation," *Frontiers in Neuroscience*, vol. 14, pp. 1–18, 2020.

[56] C. Vol, "Use of surface emg for evaluation of upper limb spasticity during botulinum toxin therapy in stroke patients," vol. 34, pp. 21–26, 2013.

[57] G. Albani, V. Cimolin, M. Galli, S. Vimercati, and D. Bar, "Use of surface emg for evaluation of upper limbspasticity during botulinum toxin therapy in stroke patients," *Functional Neurology*, vol. 31, pp. 568–574, 2010.

[58] M. J. Lueken, B. J. Misgeld, and S. Leonhardt, "Classification of spasticity affected emg-signals," *2015 IEEE 12th International Conference on Wearable and Implantable Body Sensor Networks, BSN 2015*, 2015.

[59] Y. Cha and A. Arami, "Quantitative modeling of spasticity for clinical assessment, treatment and rehabilitation," *Sensors (Switzerland)*, vol. 20, pp. 1–22, 2020.

[60] V. Dietz, M. Trippel, and W. Berger, "Reflex activity and muscle tone during elbow movements in patients with spastic paresis," *Annals of Neurology*, vol. 30, pp. 767–779, 1991.

[61] A. Albu-Schaffer, C. Ott, and G. Hirzinger, "A passivity based cartesian impedance controller for flexible joint robots-part ii: Full state feedback, impedance design and experiments," *IEEE International Conference on Robotics and Automation, 2004. Proceedings. ICRA'04. 2004*, vol. 3, pp. 2666–2672, 2004.

[62] A. Albu-Schäffer, C. Ott, and G. Hirzinger, "A unified passivity-based control framework for position, torque and impedance control of flexible joint robots," *The international journal of robotics research*, vol. 26, pp. 23–39, 2007.

[63] J. Maples and J. Becker, "Experiments in force control of robotic manipulators," *Proceedings. 1986 IEEE International Conference on Robotics and Automation*, vol. 3, pp. 695–702, 1986.

[64] N. Hogan, "Impedance control: An approach to manipulation: Part i—theory," 1985.

[65] W. S. Newman, "Stability and performance limits of interaction controllers," 1992.

[66] D. E. Whitney, "Force feedback control of manipulator fine motions," 1977.

[67] V. Gullapalli, R. A. Grupen, and A. G. Barto, "Learning reactive admittance control.," *ICRA*, pp. 1475–1480, 1992.

[68] C. Ott and Y. Nakamura, "Base force/torque sensing for position based cartesian impedance control," *2009 IEEE/RSJ International Conference on Intelligent Robots and Systems*, pp. 3244–3250, 2009.

[69] P. Lammertse, "Admittance control and impedance control-a dual," *FCS Control Systems*, vol. 13, 2004.

[70] R. J. Adams and B. Hannaford, "Stable haptic interaction with virtual environments," *IEEE Transactions on Robotics and Automation*, vol. 15, pp. 465–474, 1999.

[71] C. Ott, R. Mukherjee, and Y. Nakamura, “Unified impedance and admittance control,” *2010 IEEE international conference on robotics and automation*, pp. 554–561, 2010.

[72] R. J. Adams and B. Hannaford, “Control law design for haptic interfaces to virtual reality,” *IEEE Transactions on Control Systems Technology*, vol. 10, pp. 3–13, 2002.

[73] E. L. Faulring, K. M. Lynch, J. E. Colgate, and M. A. Peshkin, “Haptic display of constrained dynamic systems via admittance displays,” *IEEE Transactions on Robotics*, vol. 23, pp. 101–111, 2007.

[74] Y. Yokokohji, R. L. Hollis, and T. Kanade, “What you can see is what you can feel-development of a visual/haptic interface to virtual environment,” *Proceedings of the IEEE 1996 Virtual Reality Annual International Symposium*, pp. 46–53, 1996.

[75] D. Surdilovic, “Contact stability issues in position based impedance control: Theory and experiments,” *Proceedings of IEEE International Conference on Robotics and Automation*, vol. 2, pp. 1675–1680, 1996.

[76] Y. Zimmermann, A. Forino, R. Riener, and M. Hutter, “Anyexo: A versatile and dynamic upper-limb rehabilitation robot,” *IEEE Robotics and Automation Letters*, vol. 4, pp. 3649–3656, 2019.

[77] L. Zhang, S. Guo, and Q. Sun, “Development and assist-as-needed control of an end-effector upper limb rehabilitation robot,” *Applied Sciences*, vol. 10, p. 6684, 2020.

[78] N. Hogan, H. I. Krebs, J. Charnnarong, P. Srikrishna, and A. Sharon, “Mitmanus: a workstation for manual therapy and training. i,” *[1992] Proceedings IEEE International Workshop on Robot and Human Communication*, pp. 161–165, 1992.

[79] J. Patton, D. A. Brown, M. Peshkin, J. J. Santos-Munné, A. Makhlin, E. Lewis, E. J. Colgate, and D. Schwandt, “Kineassist: design and development of a robotic overground gait and balance therapy device,” *Topics in stroke rehabilitation*, vol. 15, pp. 131–139, 2008.

[80] R. C. Loureiro and W. S. Harwin, “Reach grasp therapy: Design and control of a 9-dof robotic neuro-rehabilitation system,” *2007 IEEE 10th International Conference on Rehabilitation Robotics, ICORR’07*, vol. 00, pp. 757–763, 2007.

[81] A. H. A. Stienen, J. G. McPherson, A. C. Schouten, and J. P. A. Dewald, "The act-4d: a novel rehabilitation robot for the quantification of upper limb motor impairments following brain injury," *2011 IEEE International Conference on Rehabilitation Robotics*, pp. 1–6, 2011.

[82] A. Haddadi, *Stability, performance, and implementation issues in bilateral teleoperation control and haptic simulation systems.* Queen's University (Canada), 2012.

[83] D. A. Lawrence, "Stability and transparency in bilateral teleoperation," *IEEE transactions on robotics and automation*, vol. 9, pp. 624–637, 1993.

[84] D. Lawrence and R. Stoughton, "Position-based impedance control-achieving stability in practice," *Guidance, Navigation and Control Conference*, p. 2265, 1987.

[85] S. P. Buerger and N. Hogan, "Complementary stability and loop shaping for improved human–robot interaction," *IEEE Transactions on Robotics*, vol. 23, pp. 232–244, 2007.

[86] H. Wang, F. Patota, G. Buondonno, M. Haendl, A. D. Luca, and K. Kosuge, "Stability and variable admittance control in the physical interaction with a mobile robot," *International Journal of Advanced Robotic Systems*, vol. 12, p. 173, 2015.

[87] F. Augugliaro and R. D'Andrea, "Admittance control for physical human-quadrocopter interaction," *2013 European Control Conference (ECC)*, pp. 1805–1810, 2013.

[88] E. Colgate and N. Hogan, "An analysis of contact instability in terms of passive physical equivalents," *Proceedings, 1989 international conference on robotics and automation*, pp. 404–409, 1989.

[89] G. Raisbeck, "A definition of passive linear networks in terms of time and energy," *Journal of Applied Physics*, vol. 25, pp. 1510–1514, 1954.

[90] B. Willaert, B. Corteville, D. Reynaerts, H. V. Brussel, and E. B. V. Poorten, "Bounded environment passivity of the classical position-force teleoperation controller," *2009 IEEE/RSJ International Conference on Intelligent Robots and Systems*, pp. 4622–4628, 2009.

[91] Z. Li, N. G. Tsagarakis, and D. G. Caldwell, "A passivity based admittance control for stabilizing the compliant humanoid coman," *2012 12th IEEE-RAS International Conference on Humanoid Robots (Humanoids 2012)*, pp. 43–49, 2012.

[92] S. R.J., L. J., R. S., S. P., S. R., R. T., C. S.C., B. J.E., and R. D.J., "Automating arm movement training following severe stroke: Functional exercises with quantitative feedback in a gravity-reduced environment," *IEEE Transactions on Neural Systems and Rehabilitation Engineering*, vol. 14, pp. 378–389, 2006.

[93] F. Dimeas, P. Koustoumpardis, and N. Aspragathos, "Admittance neurocontrol of a lifting device to reduce human effort," *Advanced Robotics*, vol. 27, pp. 1013–1022, 2013.

[94] J. M. Schimmels and M. A. Peshkin, "The robustness of an admittance control law designed for force guided assembly to the disturbance of contact friction," *Proceedings 1992 IEEE International Conference on Robotics and Automation*, pp. 2361–2362, 1992.

[95] C. R. Carignan and J. A. Smith, "Manipulator impedance accuracy in position-based impedance control implementations," *Proceedings of the 1994 IEEE International Conference on Robotics and Automation*, pp. 1216–1221, 1994.

[96] R. Colbaugh and K. Glass, "Simulation studies in manipulator impedance control," *1992 American Control Conference*, pp. 2941–2946, 1992.

[97] B. Heinrichs, N. Sepehri, and A. B. Thornton-Trump, "Position-based impedance control of an industrial hydraulic manipulator," *IEEE Control Systems Magazine*, vol. 17, pp. 46–52, 1997.

[98] M. Pelletier and M. Doyon, "On the implementation and performance of impedance control on position controlled robots," *Proceedings of the 1994 IEEE International Conference on Robotics and Automation*, pp. 1228–1233, 1994.

[99] V. Duchaine and C. M. Gosselin, "General model of human-robot cooperation using a novel velocity based variable impedance control," *Second Joint EuroHaptics Conference and Symposium on Haptic Interfaces for Virtual Environment and Teleoperator Systems (WHC'07)*, pp. 446–451, 2007.

[100] G. Aguirre-Ollinger, J. E. Colgate, M. A. Peshkin, and A. Goswami, "Active-impedance control of a lower-limb assistive exoskeleton," *2007 IEEE 10th International Conference on Rehabilitation Robotics*, pp. 188–195, 2007.

[101] M. M. Rahman, R. Ikeura, and K. Mizutani, "Investigating the impedance characteristic of human arm for development of robots to co-operate with human operators," *IEEE SMC'99 Conference Proceedings. 1999 IEEE International Conference on Systems, Man, and Cybernetics (Cat. No. 99CH37028)*, vol. 2, pp. 676–681, 1999.

[102] H. Seraji and R. Colbaugh, "Force tracking in impedance control," *The International Journal of Robotics Research*, vol. 16, pp. 97–117, 1997.

[103] J. E. Colgate and N. Hogan, "Robust control of dynamically interacting systems," *International journal of Control*, vol. 48, pp. 65–88, 1988.

[104] C. R. Carignan and K. R. Cleary, "Closed-loop force control for haptic simulation of virtual environments," 2000.

[105] J. M. Schimmels and M. A. Peshkin, "Force-assembly with friction," *IEEE Transactions on Robotics and Automation*, vol. 10, pp. 465–479, 1994.

[106] G. D. Glosser and W. S. Newman, "The implementation of a natural admittance controller on an industrial manipulator," *Proceedings of the 1994 IEEE International Conference on Robotics and Automation*, pp. 1209–1215, 1994.

[107] N. Hogan, "Controlling impedance at the man/machine interface," *1989 IEEE International Conference on Robotics and automation*, pp. 1626–1627, 1989.

[108] H. Kazerooni, "Human-robot interaction via the transfer of power and information signals," *IEEE Transactions on systems, Man, and Cybernetics*, vol. 20, pp. 450–463, 1990.

[109] M. Nambi, W. R. Provancher, and J. J. Abbott, "On the ability of humans to apply controlled forces to admittance-type devices," *Advanced Robotics*, vol. 25, pp. 629–650, 2011.

[110] S. Bhardwaj, A. A. Khan, and M. Muzammil, "Electromyography in physical rehabilitation: a review," *National Conference on Mechanical Engineering–Ideas, Innovations Initiatives*, pp. 64–69, 2016.

[111] S. H. Chen, W. M. Lien, W. W. Wang, G. D. Lee, L. C. Hsu, K. W. Lee, S. Y. Lin, C. H. Lin, L. C. Fu, J. S. Lai, J. J. Luh, and W. S. Chen, "Assistive control system for upper limb rehabilitation robot," *IEEE Transactions on Neural Systems and Rehabilitation Engineering*, vol. 24, pp. 1199–1209, 2016.

[112] W. Yu, J. Rosen, and X. Li, "Pid admittance control for an upper limb exoskeleton," *Proceedings of the 2011 American control conference*, pp. 1124–1129, 2011.

[113] P. Culmer, A. Jackson, M. C. Levesley, J. Savage, R. Richardson, J. A. Cozens, and B. B. Bhakta, "An admittance control scheme for a robotic upper-limb stroke rehabilitation system," *2005 IEEE Engineering in Medicine and Biology 27th Annual Conference*, pp. 5081–5084, 2006.

[114] M. G. Carmichael and D. Liu, "Admittance control scheme for implementing model-based assistance-as-needed on a robot," *2013 35th Annual International Conference of the IEEE Engineering in Medicine and Biology Society (EMBC)*, pp. 870–873, 2013.

[115] A. Lecours, B. Mayer-St-Onge, and C. Gosselin, "Variable admittance control of a four-degree-of-freedom intelligent assist device," *2012 IEEE international conference on robotics and automation*, pp. 3903–3908, 2012.

[116] D. Liberzon, *Switching in systems and control*, vol. 190. Springer, 2003.

[117] M. Dyck, A. Jazayeri, and M. Tavakoli, "Is the human operator in a teleoperation system passive?," *2013 World Haptics Conference (WHC)*, pp. 683–688, 2013.

[118] A. Q. L. Keemink, H. van der Kooij, and A. H. A. Stienen, "Admittance control for physical human–robot interaction," *The International Journal of Robotics Research*, vol. 37, pp. 1421–1444, 2018.

[119] S. P. Buerger and N. Hogan, "Relaxing passivity for human-robot interaction," *2006 IEEE/RSJ international conference on intelligent robots and systems*, pp. 4570–4575, 2006.

[120] K. Hashtrudi-Zaad and S. E. Salcudean, "Analysis of control architectures for teleoperation systems with impedance/admittance master and slave manipulators," *The International Journal of Robotics Research*, vol. 20, pp. 419–445, 2001.

[121] J. E. Colgate and J. M. Brown, "Factors affecting the z-width of a haptic display," *Proceedings of the 1994 IEEE International Conference on Robotics and Automation*, pp. 3205–3210, 1994.

APPENDIX A

Nomenclature

D	Mechanical admittance transfer function
ω	Physical or virtual mechanical angular velocity, frequency ($\omega_c^0, j\omega$)
H	Transfer function
τ	Physical or virtual mechanical torque
S	Controller gain
i	Electrical current
s	Laplace variable
E	Estimator / Observer
T	Time Constant
M	Mechanical impedance, physical or model
O	Related to current controller
k	Controller gains, mechanical stiffness, transmission ratio
K	Controller gains (k_p, k_i, k_d, k_a) multiplied by the transmission ratio squared
j	Imaginary constant
β	Physical or virtual mechanical damping
m	Physical or virtual mass
l	Physical or virtual radius
μ	Feed-forward inertial coefficient
ρ	Feed-forward damping coefficient
σ	EMG Envelope

APPENDIX B

Transfer Functions and Function Definitions

$$\begin{aligned} D_a(s) &= \frac{\omega}{\tau_{sen}} \\ &= \frac{D_r(H_d E_\tau [S_v + O' D'_v] + 1)}{D_r(I_{ps} + Q + 1)} \end{aligned}$$

where

$$Q(s) = H_d(O_{fb} E_\omega k_r + S_v E_\tau M_{ps} - O' D_v \delta_Z)$$

$$O'(s) = O_{fb} + O_{ff}$$

$$D'_v(s) = D_v(s) k_r$$

$$\delta_Z(s) = E_\alpha \widehat{M_{ps}} - E_\tau M_{ps}$$

$$H_d(s) = H H_i k_r$$

$$D_r(s) = \frac{1}{I_r s + \beta_r}$$

which consists of the following -

$$O_{fb}(s) = k_p + \frac{k_i}{s} + \frac{k_d s}{T_c s + 1}$$

$$O_{ff}(s) = \mu_{ff} s + \rho_{ff}$$

$$I_r = \frac{1}{3} m_r l_r^3$$

$$I_v = \frac{1}{3} m_v l_v^3$$

$$I_{ps} = \frac{1}{3} m_{ps} l_{ps}^3$$

$$D_{ps}(s) = I_{ps} s, \widehat{D_{ps}}(s) = \frac{\mu_c s}{T_c s + 1}$$

$$H_{zoh}(s) = \frac{1 - e^{sT_s}}{sT_s}, H_i(s) = k_\tau \frac{e^{-sT_d}}{T_i s + 1}$$

$$D_v(s) = \frac{k_a s^2 + s}{I_v s^2 + \beta_v s + k_v}$$

$$E_\omega(s) = \frac{1}{T_\omega s + 1},\ E_\tau(s) = \frac{1}{T_\tau s + 1},\ E_\alpha(s) = \frac{1}{T_a s + 1}$$

APPENDIX C

Stability and Passivity

Naïve feedback

$$D_a(s) = \frac{1}{s}\frac{I_v s^2 + K_p s + K_i}{a_2 s^2 + a_1 s + a_0}$$

With $a_2 = (I_r + I_{ps})\, I_v$, $a_1 = (K_p + \beta_r)\, I_v + K_p I_{ps}$,

$a_0 = K_i\,(I_v + I_{ps})$, $K_p = k_p k_r^2$ and $K_i = k_i k_r^2$

$$D_a\,(j\omega) = \frac{(I_v\omega^2 - K_i) - jK_p\omega}{a_1\omega^2 + j\,(a_2\omega^3 - a_0\omega)} = \frac{\eta_a\,(j\omega)}{\delta_a\,(j\omega)}$$

which then makes the real condition

$$R\{\eta_a\}\,R\{\delta_a\} + J\{\eta_a\}\,J\{\delta_a\} \geq 0,\ \forall\omega$$

$$c_1\omega^4 + c_2\omega^2 \ \geq 0,\ \forall\omega$$

$$c_1 = (K_p + \beta_r)\, I_v^2 - K_p I_r I_v$$

$$c_2 = -K_i \beta_r I_v$$

In order to reach passivity, we need c_1 and $c_2 \geq 0$. Removing I_v by dividing leads us to equations (4.9) and (4.10).

Naïve accommodation control

We combine equations (4.5), (4.7), and (4.8) with a new D_v in the form of $\frac{1}{\beta_v}$ to get the apparent dynamic function -

$$D_a(s) = \frac{(K_p + \beta_v)\, s + K_i}{\beta_2 s^2 + ([K_p + \beta_r]\,\beta_v + K_i I_{ps})\, s + \beta_v K_i}$$

where $\beta_2 = (I_r + I_{ps})\,\beta_v + K_p I_{ps}$, similarly to the previous section, as well as $s = j\omega$, getting the following conditions -

$$d_1\omega^2 + d_2 \geq, \ \forall\omega$$

$$d_1 = (K_p + \beta_v)\,(K_p + \beta_r)\,\beta_v - K_i I_r \beta_v$$

$$d_2 = b_v K_i^2$$

In order to meet passivity, we need $d_1 \geq 0$ and $d_2 \geq 0$. We know that $\beta_v \geq 0$ from d_2, leading to the passivity condition in the text.

Naïve stiffness control

We copy the approach from the previous accommodation control but with $D_v(s) = \frac{s}{k_v}$

$$D_a(s) = \frac{K_r s^2 + (K_i + k_v)\,s}{K_p I_{ps} s^3 + \gamma_2 s^2 + (K_p \beta_r)\,k_v s + K_i k_v}$$

where $\gamma_2 = (I_r + I_{ps})\,k_v + K_i I_{ps}$, which is stable for positive real conditions. The passivity conditions then become -

$$e_1\omega^4 + e_2\omega^2 \geq 0, \ \forall\omega$$

$$e_1 = K_p k_v I_r$$

$$e_2 = (K_p + \beta_r)\,k_v^2 + K_i \beta_r k_v$$

Element combinations

Combining the naïve accommodation and stiffness parameters to find passivity, we make the new virtual dynamics into -

$$D_v(s) = \frac{s}{I_v s^2 + \beta_v s + k_v}$$

which then combines with the controller to make the apparent dynamics -

$$D_a(s) = \frac{I_v s^3 + (\beta_v + K_p)\, s^2 + (K_i + k_v)\, s}{I_r I_v s^4 + \varphi_3 s^3 + \varphi_2 s^2 + \varphi_1 s + K_i k_v}$$

Where $\varphi_3 = \beta_r I_v + \beta_v I_r + K_p I_v$, $\varphi_2 = \beta_r \beta_v + \beta_v K_p + K_i I_v + k_v I_r$, and $\varphi_1 = \beta_v K_i + \beta_r k_v + K_p k_v$. While this system is not necessarily stable for positive real parameters, we must use the Routh array to determine the passivity condition -

$$\begin{aligned}
&\beta_v\left(\beta_r + K_p\right)\left(\left[\beta_r^2 + K_p^2\right] k_v I_v + \left[\beta_r \beta_v + \beta_v K_p + K_i I_v\right] K_i I_v ...\right.\\
&+ \left[\beta_r \beta_v + \beta_v K_p + k_v I_r\right] k_v I_r + 2\beta_r K_p k_v I_v + \beta_v^2 K_i I_r ...\\
&\geq 2\left(\beta_r + K_p\right)\left(\beta_v K_i k_v I_r I_v\right)
\end{aligned}$$

which imparts an upper limit on K_i. Changing $s = j\omega$ as before we get -

$$\lambda_1 \omega^6 + \lambda_2 \omega^4 + \lambda_3 \omega^2 \geq 0,\ \forall \omega$$

$$\lambda_1 = \beta_r I_v^2 + K_p I_v^2 - K_p I_r I_v$$

$$\begin{aligned}
\lambda_2 = \beta_r \beta_v^2 + \beta_v K_p^2 + \beta_v^2 K_p + \beta_r \beta_v K_p - \beta_r K_i I_v - \beta_v K_i I_r ...\\
-2\beta_r k_v I_v + K_p k_v I_r - 2K_p k_v I_v
\end{aligned}$$

$$\lambda_3 = \beta_v K_i^2 + \beta_r k_v^2 + K_p k_v^2 + \beta_r K_i k_v$$

$$\delta_{mk} = -2\left(K_p + \beta_r\right) k_v I_v$$

We can see the congruence to (4.9) and therefore $\delta_1 = c_1$, $\delta_2 = d_2 + e_2$, and $\delta_3 = c_1 + d_1 + e_1$ from the naive feedback passivity condition. This shows that (4.9) is unchanging when adding haptic elements.

Consideration 1 - Torque signal filtering

We filter the torque with the low-pass filter -

$$E_\tau(s) = \frac{1}{T_f s + 1}$$

which changes the virtual dynamics to -

$$D'_v(s) = D_v E_\tau = \frac{1}{I_v s}\frac{1}{T_f s + 1} = \frac{1}{T_f I_v s^2 + I_v s}$$

Setting $k_i = 0$ because we know the admittance controller has the positive real requirement, we get apparent dynamics -

$$D_a(s) = \frac{1}{s}\frac{I_v T_f s^2 + I_v s + K_p}{h_2 s^2 + h_1 s + (K_p + \beta_r) I_v + K_p I_{ps}}$$

with $h_1 = ([K_p + \beta_r] T_f + I_r + I_{ps}) I_v$ and $h_2 = (I_r + I_{ps}) T_f I_v$, yielding the conditions -

$$n_1 \omega^4 + n_2 \omega^2 \geq 0, \ \forall \omega$$

$$n_1 = (K_p + \beta_r) I_v^2 T_f^2$$

$$n_2 = (K_p + \beta_r) I_v^2 - K_p I_v (I_r + [K_p + \beta_r] T_f)$$

Consideration 2 - Feed-forward control

Changing the torque control equation to include feed-forward control -

$$\tau_c(s) = k_r \left(\frac{k_p s + k_i}{s} [\omega_d - k_r \omega] + [\mu_{ff} s + \rho_{ff}] \omega_d + S_v \tau_{sen} \right)$$

which combined with changing the virtual dynamics to $D_v(s) = \frac{1}{I_v s}$, results in the apparent dynamics

$$D_a(s) = \frac{1}{s}\frac{(\mu_{ff} k_r^2 + [1 + S_v k_r] I_v) s^2 + (\rho_{ff} k_r^2 + K_p) s + K_i}{f_2 s^2 + f_1 s + f_0 s}$$

with $f_2 = \mu_{ff} k_r^2 I_{ps} + (I_r + I_{ps}) I_v$, $f_1 = (K_p + \beta_r) I_v + (\rho_{ff} k_r^2 + K_p) I_{ps}$, and $f_0 = (I_v + I_{ps}) K_i$. This is always stable for positive parameters. Changing $s = j\omega$ as before we get -

$$g_1 \omega^4 + g_2 \omega^2 \geq 0, \ \forall \omega$$

$$
\begin{aligned}
g_1 = &\left(S_v k_r + 1\right)\left(K_p + \beta_r\right) I_v^2 \\
&- \left(K_p + \rho_{ff} k_r^2\right) I_r I_v + \left(K_p + \beta_r\right) \mu_{ff} k_r^2 I_v
\end{aligned}
$$

$$g_2 = \left(\rho_{ff} k_r^2 - \beta_r\right) K_i$$

which requires $g_1 \geq 0$ and $g_2 \geq 0$. We can simplify these down to (4.12) and (4.13) by dividing g_1 by I_v. The result shows that using this method effectively reduces the apparent robot inertia seen by the controller.

Consideration 3 - Virtual damping

We introduce virtual damping by changing the virtual dynamics to -

$$D_v(s) = \frac{1}{I_v s + \beta_v}$$

which results in the apparent dynamics

$$D_a(s) = \frac{I_v s^2 + \left(K_p + \beta_v\right) s + K_i}{\left(I_r + I_{ps}\right) I_v s^3 + t_2 s^2 + t_1 s + K_i \beta_r}$$

with $t_2 = \left(I_r + I_{ps}\right)\left(K_p + \beta_v\right) + \beta_r I_v$, $t_1 = \left(I_v + I_{ps}\right) K_i \left(K_p + \beta_r\right) \beta_v$, and $t_2 t_1 \geq \left(I_r + I_{ps}\right) I_v K_i \beta_r$. Assessing the characteristic equation, we can say it's stable when uncoupled based on the condition $t_2 t_1 \geq (I_r + I_{ps}) I_v K_i \beta_r$ is always true for positive variables, resulting in stable poles. Changing $s = j\omega$ as before we get -

$$u_1 \omega^4 + u_2 \omega^2 + u_3 \geq 0, \ \forall \omega$$

$$u_1 = \left(K_p I_v - K_p I_r + \beta_r I_v\right) I_v$$

$$u_2 = \beta_v \left(K_p + \beta_v\right)\left(K_p + \beta_r\right) - K_i \left(\beta_r I_v + \beta_v I_r\right)$$

$$u_3 = K_i \beta_v$$

As prior, we require that $u_1 \geq 0$, $u_2 \geq 0$, and the passivity conditions are discussed in the text.

Consideration 4 - Modification of angular velocity reference

We introduce add the acceleration phase lead by changing -

$$D_v'(s) = \frac{k_a s + 1}{I_v s}$$

which results in the apparent dynamics

$$D_a(s) = \frac{1}{s}\frac{(K_p k_a + I_v)\, s^2 + (K_p + K_i k_a)\, s + K_i}{v_2 s^2 + v_1 s + (I_v + I_{ps})\, K_i}$$

with $v_2 = I_r I_v + I_{ps}\,(I_v + K_p k_a)$, and $v_1 = (K_p + \beta_r)\, I_v + (K_p + K_i k_a)\, I_{ps}$. Changing $s = j\omega$ as before we get -

$$w_1 \omega^4 + w_2 \omega^2 \geq 0,\ \forall \omega$$

$$w_1 = (K_p + \beta_r)\, I_v^2 + \left(\left[K_p^2 + \beta_r K_p - K_i I_r\right] k_a - k_p I_r\right) I_v$$

$$w_2 = (k_a K_i - \beta_r)\, K_i I_v$$

As prior, we require that $w_1 \geq 0$, $w_2 \geq 0$, and the passivity conditions are discussed in the text.

Consideration 5 - Velocity controller bandwidth

We have the apparent admittance -

$$D_a(s) = \frac{1}{s}\frac{I_v T_d s^3 + x_2' s^2 + (K_p + K_i T_d)\, s + K_i}{s\,(I_r + I_{ps})\, I_v T_d s^3 + x_2 s^2 + x_1 s + x_0}$$

with

$x_2' = I_v + K_d + K_p T_d$,$x_2 = (I_r + I_{ps})\, I_v + (I_v + I_{ps})\, K_d + ([K_p + \beta_r]\, I_v + K_p I_{ps})\, T_d$, $x_1 = (K_p + \beta_r)\, I_v + K_p I_{ps} + K_i T_d\,(I_v + I_{ps})$, and $x_0 = (I_v + I_{ps})\, K_i$. Using the Routh array we extract - $x_2 x_1 \geq (I_r + I_{ps})\, I_v x_0$ and we can expect this to hold up for positive parameters. Changing $s = j\omega$ as before we get -

$$y_1 \omega^6 + y_2 \omega^4 + y_3 \omega^2 \geq 0,\ \forall \omega$$

$$y_1 = \left(K_d + \left[K_p + \beta_r\right] T_d\right) T_d I_v^2 - \left(K_p T_d + K_d\right) I_r I_v T_d$$

$$y_2 = \left(K_p + \beta_r\right) I_v^2 + \left(\beta_r \left[K_d - K_i T_d^2\right] - K_p I_r\right) I_v$$

$$y_3 = -\beta_r K_i I_v$$

Given the requirement for $y_1 \geq 0$, $y_2 \geq 0$, and $y_3 \geq 0$ along with the positive parameter condition, we can say the system will not be passive with a positive integral gain. The passivity conditions are discussed in detail in the text.

Consideration 6 - Complex gain

Following the logic and setup of the feed-forward-enabled control algorithm, we include the virtual dynamics $D_v(s) = \frac{1}{I_v s}$ and include the complex gain loop in the form $S_v(s) = \mu_{sv} s + \rho_{sv}$, resulting in the apparent dynamics

$$D_a(s) = \frac{1}{s} \frac{\left(\mu_{ff} k_r^2 + \left[1 + \mu_{sv} k_r\right] I_v\right) s^2 + \left(\rho_{ff} k_r^2 + K_p\right) s + K_i}{f_2 s^2 + f_1 s + f_0}$$

with $f_2 = \mu_{ff} k_r^2 I_{ps} + \left(I_r + I_{ps}\right) I_v$, $f_1 = \left(K_p + \beta_r\right) I_v + \left(\rho_{ff} k_r^2 + K_p\right) I_{ps}$, and $f_0 = \left(I_v + I_{ps}\right) K_i$. This is always stable for positive parameters. Changing $s = j\omega$ as before we get -

$$g_1 \omega^4 + g_2 \omega^2 \geq 0, \;\; \forall \omega$$

$$\begin{aligned} g_1 = &\left(\mu_{sv} s + \rho_{sv} k_r + 1\right) \left(K_p + \beta_r\right) I_v^2 \\ &- \left(K_p + \rho_{ff} k_r^2\right) I_r I_v + \left(K_p + \beta_r\right) \mu_{ff} k_r^2 I_v \end{aligned}$$

$$g_2 = \left(\rho_{ff} k_r^2 - \beta_r \rho_{sv}\right) K_i$$

which requires $g_1 \geq 0$ and $g_2 \geq 0$. We can surmise the g_2 can be simplified to $\rho_{ff} k_r^2 \geq \beta_r \rho_{sv}$ which shows the condition for passivity once again would highly benefit from a low gear ratio, as an increase in gear ratio would require a higher ρ_{sv} or B_r.

VITA

RODRIGO NICOLAS RAMON

August 21, 1989	Born, Miami, Florida
2016	B.S., Electrical Engineering Florida International University Miami, Florida
2020	M.S., Electrical Engineering Florida International University Miami, Florida

PUBLICATIONS AND PRESENTATIONS

Ramon, R., Bai, O. (2017). *Efficient upper limb joint displacement modeling using EMG signal for driving an assistive SCARA*. 2017 IEEE International Conference on Mechatronics and Automation (ICMA), 1538–1542.

Ramon, R., Bai, O. (2019). *High-Level Parametric Gait Modeling for Assistive Robotics*. 2019 IEEE International Symposium on Measurement and Control in Robotics (ISMCR), A1-2.

Ramon, R., Nataros, C., Yi, T., Lagos, L., Avarelli, A., Bai, O. (2019). *Hotcell Worker Assistive Robotic Exoskeleton Design and Control*. 2019 IEEE International Symposium on Measurement and Control in Robotics (ISMCR), A1-3.

Ramon, R., Yi, T., Nataros, C., Garcia, C., Aravelli, A., Lagos, L., Bai, O. (2020). *Robotic Exoskeleton Design and System Control for Glovebox Operators in Nuclear Facilities*. 2020 IEEE/SICE International Symposium on System Integration (SII), 509–512.

Ramon, R., Hasan S., Bai, O. (2022). *Accurate torque modulation in rehabilitation robotics using admittance control*. IEEE Transactions on Neurorehabilitation. (Submitted - Pending Review)